DOKUZ EYLÜL UNIVERSITY

GRADUATE SCHOOL OF NATURAL AND APPLIED SCIENCES

INVESTIGATION OF THE PETROGRAPHIC, MINERALOGICAL AND GEOCHEMICAL COMPOSITION OF THE COAL FROM THE CURRENT MUĞLA-YATAĞAN COAL FIELD DRILLING DATA

by

Burcu ERECEK

February, 2024

İZMİR

INVESTIGATION OF THE PETROGRAPHIC, MINERALOGICAL AND GEOCHEMICAL COMPOSITION OF THE COAL FROM THE CURRENT MUĞLA-YATAĞAN COAL FIELD DRILLING DATA

The Thesis Submitted to the
Graduate School of Natural and Applied Sciences of Dokuz Eylül University
In Partial Fulfillment of the Requirements for the Degree of Master of Science
in Geological Engineering, Economic Geology Program

by
Burcu ERECEK

February 2024
İZMİR

M.SC THESIS EXAMINATION RESULT FORM

We have read the thesis entitled **"INVESTIGATION OF THE PETROGRAPHIC, MINERALOGICAL AND GEOCHEMICAL COMPOSITION OF THE COAL FFROM THE CURRENT MUĞLA-YATAĞAN COAL FIELD DRILLING DATA"** completed by **BURCU ERECEK** under supervision of **ASSOCIATE PROF. DR. MEHMET AKBULUT** and we certify that in our opinion it is fully adequate, in scope and in quality, as a thesis for the degree of Master of Science.

Assoc. Prof. Dr. Mehmet AKBULUT

Supervisor

Prof. Dr. Tolga OYMAN

Jury Member

Prof. Dr. Fikret SUNER

Jury Member

Prof.Dr. Okan FISTIKOĞLU
Director
Graduate School of Natural and Applied Sciences

ACKNOWLEDGEMENTS

Firstly, I would like to thank my thesis supervisor Associate Prof. Dr. Mehmet AKBULUT and my esteemed second thesis supervisor, Prof. Dr. em, Kimon CHRISTANIS for sharing their knowledge and experience with me in the field, in the laboratory and throughout the thesis.

I would like to thank Fatih TURAN and Ziya ÇOBAN from Dokuz Eylül University, Department of Mining Engineering for their help and experience in all processes of proximate analysis.

Esteemed Prof. Dr. Hülya İNANER and Prof. Dr. Tolga OYMAN are thanked for their support throughout my undergraduate/graduate education. I would like to express my gratitude to Zeynep BÜÇKÜN for her patience and guidance during evaluation of the analysis results. I would also like to thank, Itumeleng MATLALA for her assistance in the analysis and evaluation of Micro-Raman Spectroscopy data.

Işık HACIMUSTAFAOĞLU, who supported me throughout my field, laboratory and microscope studies are appreciated.

Cemal DOĞANALP, Bayram ÖZKAN and Yavuz TERZİOĞLU are thanked for their patience and understanding approach throughout the thesis processing and for sharing their experiences with me.

I thank my teammates Ali Erdem BAKKALBAŞI, Yekta Nur ÇELİK and Alican KOCA for their understanding and support.

Finally, I would like to express my gratitude to my dear mother, Semiha USLU, who supported me financially and emotionally throughout my school life, and to my father Ertuğrul ERECEK, and my sister Duygu ERECEK. I thank Erhan Berk ÇOLAKOĞLU for his support.

Burcu ERECEK

ABSTRACT

This study aims to report and evaluate the petrographic, mineralogical and geochemical composition of four samples taken from the B-22 borehole core obtained from the newly discovered coalfield located between Şahinler and Bozüyük in the southwest of Yatağan district of Muğla province.

The results of the proximate analysis completed earlier from the samples were as follows; the average total moisture is 5.28%; the ash yield 35.38% (dry basis), volatile matter yield 39.23% (dry basis); fixed carbon yield 25.39% (dry basis); the total sulfur content 5.47% (dry basis); the net calorific value 16.08 MJ/kg and the gross calorific value is 16.89 MJ/kg. The ash value of sample number 4 is 71.50%; hence, it is not considered as coal. The sample is classified as a carbonaceous rock, therefore being not included from the averaged values.

The result of maceral analysis and reflectance measurements (in Appendix II) on whole rock basis are as follows: the average telohuminite content is 14.67 vol.%, the average detrohuminite 50,67%, the average gelohuminite 11.34%, the average liptinite (mainly sporinite, alginite and cutinite) 5.67%, the average inertinite (mainly fusinite, funginite and micrinite) 3.67%, and the average mineral content is 14% (again, sample 4 is excluded from the average calculations). Huminite group macerals are common, while the inertinite and liptinite macerals are rare and the mineral matter content varies.

Recently laser micro-Raman Spectroscopy is widely used to determine the structural properties of carbonaceous materials. Thus, a set of micro-Raman spectroscopic data has been acquired from huminite and inertinite macerals. The micro-Raman work was performed on one sample only. The micro-Raman data obtained were evaluated using three different Raman Spectroscopy software (IFORS (Python software), SpectraGryph and OriginPro) in order to compare the processed results. According to the results, the values of the D1 band of the fusinite macerals vary between 1345 and 1397 cm^{-1} with an average of 1375.17 cm^{-1}. The D1 band values of ulminites range between 1356-1362 cm^{-1} with an average of 1359 cm^{-1}. The values of the G band range between 1587-1609 cm^{-1} in fusinites and the average is 1598.75 cm^{-1}. The average D1 and G bands obtained are within the range of values of

the coal spectrum obtained by Tuinstra and Koenig (1970), and Friedel and Carlson (1971). Data obtained from Micro-Raman Spectroscopy encourage further inquiry of the method as a complementary method in low-rank coals.

Keywords: Lignite, coal petrology, maceral, micro-Raman spectroscopy, Yatağan, Muğla.

ÖZ

Bu çalışma; Muğla ili Yatağan ilçesinin güneybatısında, Şahinler-Bozüyük arasında yer alan yeni bulunan kömür sahasında Yatağan Termik Santrali içerisinde yapılan B-22 sondajından alınan dört adet örneğin petrografik, mineralojik ve jeokimyasal kompozisyonu rapor edilerek değerlendirmesi amaçlanmıştır.

Örneklerden önceden yapılan kaba analiz sonuçları şu şekildedir; ortalama toplam nem içeriği %5,28 (kuru bazda), kül içeriği %35,38 (kuru bazda), uçucu madde içeriği %39,23 (kuru bazda), sabit karbon içeriği %25,39 (kuru bazda), toplam kükürt içeriği %5,47 (kuru bazda), net kalorifik değer 16,08 MJ/kg ve brüt kalorifik değer 16,89 MJ/kg'dır. Dört numaralı örneğin kül değeri 71,50%'dir; bu nedenle kömür olarak kabul edilmemiştir. Örnek, yüksek karbon içeriğine sahip kayaç olarak sınıflandırılmıştır ve bu sebeple ortalama değerler hesaplanırken dahil edilmemiştir.

Tüm kayaç bazında yapılan maseral analiz ve reflektans ölçümlerinin sonuçları şu şekildir; ortalama telohüminit içeriği hacimce %14,67; ortalama detrohüminit içeriği %50,67; ortalama jelohüminit %11,34; ortalama liptinit (sporinit, aliginit ve kütinit) %5,67 (tüm kayaç bazında), ortalama inertinit (fusinit, funginit ve mikrinit) %3,67; ortalama mineral içeriği %14 olarak hesaplanmıştır (yine ortalama hesabı yapılırken dört numaralı örnek hesaplamalara dahil edilmemiştir). Huminit grubu maserallerin yaygın olduğu, inertinit ve liptinit grubu maserallerin ise nadir olduğu ve minerallerin çeşitlilik gösterdiği sonucuna varılmıştır.

Lazer micro-Raman Spektroskopisi günümüzde karbonlu malzemelerin yapısal özelliklerini belirlemek için yaygın olarak kullanılmaktadır. Bu sebeple hüminit ve inertinit maserallerinde bir dizi mikro-Raman spektroskopik veri elde edilmiştir. Mikro-Raman çalışması sadece tek bir örnekte gerçekleştirilmiştir. Elde edilen micro-Raman verileri işlenen sonuçları karşılaştırmak amacıyla üç farklı Raman Spektroskopi yazılımı (IFORS (Python yazılımı), SpectraGryph ve OriginPro) kullanılarak değerlendirilmiştir. Sonuçlara göre fusinit maserallerinin D1 bandının değerleri 1345-1397 cm^{-1} arasında değişmekte olup ortalaması 1375,17 cm^{-1}'dir. Ulminitlerin D bandının değerleri 1356-1362 cm^{-1} arasında değişmekte olup ortalaması 1359 cm^{-1}'dir. G bandının değerleri fusinitlerde 1587-1609 cm^{-1}

aralığındadır ve ortalama 1598,75 cm^{-1}'dir. Elde edilen ortalama D ve G bantlarının değerleri, Tuinstra ve Koenig (1970) ve Friedel ve Carlson (1971) tarafından elde edilen kömür spektrumu değerleri aralığındadır. Mikro-Raman Spektroskopisinden elde edilen veriler, düşük dereceli kömürlerde tamamlayıcı bir yöntem olarak yöntemin daha fazla araştırılmasını teşvik etmektedir.

Anahtar Sözcükler: Linyit, kömür, maseral, mikro-Raman spektroskopisi, Yatağan, Muğla.

CONTENTS

M.SC THESIS EXAMINATION RESULT FORM ..... **ii**
ACKNOWLEDGEMENTS ..... **iii**
ABSTRACT ..... **iv**
ÖZ ..... **vi**
LIST OF FIGURES x
LIST OF TABLES xii
LIST OF PLATE xiii
CHAPTER ONE **1**
INTRODUCTION **1**
1.1. Aim of The Study 2
1.2. The Study Area 2
1.3. Previous Studies 4
CHAPTER TWO **6**
GEOLOGICAL SETTING **6**
2.1. Pre-Neogene Formations 6
2.2. Neogene Formations 7
2.3. Quaternary Formations 10
CHAPTER THREE **11**
MATERIALS AND METHODS **11**
CHAPTER FOUR **18**
RESULTS **18**
4.1. Definitions of the Studied Macerals and Maceral Subgroups and Huminite Reflectance Measurements 18
4.2 Analytical Data from Borehole B-22: The Maceral Composition and The Reflectance 22
4.3. Data from the Proximate Analysis 27
4.4. Portable X-Ray Fluorecence (PXRF) and X-Ray Diffractometer (XRD) Results 27
4.5. Micro-Raman Spectroscopy 30
CHAPTER FIVE **43**
DISCUSSIONS AND CONCLUSIONS **43**
REFERENCES 45

APPENDIX I 51
APPENDIX II 60

LIST OF FIGURES

Page

Figure 1. The location of the study area and the roughly located #B22 drillhole; the red line shows the boundary of the thermal powerplant, the dashed yellow line show the boundary of licence. 3
Figure 2. Geological map of Yatağan Basin (Ünal, 1989; Bulut et al., 2001). 7
Figure 3. Generalized lithostratigraphic section of the Muğla-Yatağan lignite basin (after Gürsoy et al., 1993, İnaner, 1994). 8
Figure 4. The lithostratigraphic section of the B-22 core with the sampling depths (Erecek, 2020). 12
Figure 5. OLYMPUS DELTA Premium DP-6000 (Portable-XRF Measuring Device). 15
Figure 6. Maceral analysis of samples with LEICA DM 4500 P brand microscope. 16
Figure 7. View of the Renishaw Raman Spectroscopy instrument. 17
Figure 8. Simplified pathways of maceral genesis (ICCP course Organic Petrology notes, 2022). 19
Figure 9. Rank determinations of studied coal samples in accordance to the German and North American classifications (after Taylor et al., 1998). Transparent greenfields denotes the ranges obtained and compiled from the coal samples..... 24
Figure 10. Coal rank determination according to the ECE-UN (1998) scheme. Transparent greenfield denotes spread of the samples. 25
Figure 11. The ABC ternary plot of the Yatağan coal samples (after Mukhopadhyay, 1989). 26
Figure 12. XRD spectrum of the sample 3 Abbreviations denotes,Qz: quartz, M: mica, Kln: kaolinite, Chl:chlorite, Sm: Smectite, Ca: calcite, Kfs: potassium feldspar, Pl: plagioclase, Bass: Basaluminite (Felsőbányaite). 29
Figure 13. Example of Raman parameters and non-deconvoluted spectrum; Parameters of interest described here are saddle index (SI), Raman band separation (RBS), G-band/function full-width at half-maximum (G-FWHM), D band/function full-width at half-maximum (D-FWHM), scaled spectrum area (SSA) (Henry et al., 2019). 31
Figure 14. Examples of unprocessed visuals of the D- and G-band curves of 22_1_13 and 22_1_13_1 ulminite maceral. Visuals are illustrated via SpectraGryph software. 34

Figure 15. Examples of the D- and G-band curves of 22_1_13 and 22_1_13_1 ulminite maceral. Deconvolution curves and visuals are illustratedusing Python based IFORS software. 35
Figure 16. Examples of the D- and G-band curves of 22_1_13 and 22_1_13_1 ulminite maceral. Deconvolution curves and visuals are illustrated via generated using the OriginPro software. 36
Figure 17. Examples of unprocessed D- and G-band curves of 22_1_8 and 22_1_19 fusinite maceral. Visuals are from SpectraGryph software. 37
Figure 18. Examples of the D- and G-band curves of 22_1_8 and 22_1_19 fusinite maceral. Deconvolution curves and visuals aregenerated using the Python based IFORS software 38
Figure 19. Examples of the D- and G-band curves of 22_1_8 and 22_1_19 fusinite maceral. Deconvolution curves and visuals generated using the OriginPro 2023 software. 39
Figure 20. Area D1/Area G versus Reflectance (%Ro) plot. 40
Figure 21. Intensity D1/Intensity G versus Reflectance (%Ro) plot. 41
Figure 22. Graph of the Reflectance (%Ro) versus D1 FWHM (FWHM=Width at half height of the peak (cm^{-1})). 41
Figure 23. Graph of the Reflectance (%Ro) versus G FWHM (FWHM=Width at half height of the peak (cm^{-1})). 42

LIST OF TABLES

Page

Table 1. Huminite group macerals (modified from Ward, 1984). 19
Table 2. Liptinite group macerals (modified from Ward, 1984). 20
Table 3. Inertinite group macerals (modified from Ward, 1984). 21
Table 4. Group/sub-group analysis results of macerals. 23
Table 5. XRD diagrams of the sample. 28
Table 6. Raman parameters from the analytical data obtained via deconvolution of the curves of micro-Raman spectra (Abbreviations FWHM=Width at half height of the peak (cm^{-1})). 33

LIST OF PLATE

Page

Plate 1. Photomicrographs of sample #1 under incident white light and blue-light excitation, oil immersion, 500X total magnification. 52
Plate 2. Photomicrographs of sample #1 and #2 under incident white light and blue-light excitation, oil immersion, 500X total magnification. 54
Plate 3. Photomicrographs of sample #3 and #4 under incident white light and blue-light excitation, oil immersion, 500X total magnification. 56
Plate 4. Photomicrographs of sample #4 under incident white light and blue-light excitation, oil immersion, 500X total magnification. 58
Plate 5. D1 and G peak parameters of samples from SpectraGryph. 61
Plate 6. D1 and G peak parameters of samples from SpectraGryph. 62
Plate 7. D1 and G peak parameters of samples from SpectraGryph. 63
Plate 8. D1 and G peak parameters of samples from IFORS. 64
Plate 9. D1 and G peak parameters of samples from IFORS. 65
Plate 10. D1 and G peak parameters of sample from IFORS. 66
Plate 11. D1 and G peak parameters of samples from OriginPro. 67
Plate 12. D1 and G peak parameters of samples from OriginPro. 68
Plate 13. D1 and G peak parameters of samples from OriginPro. 69
Plate 14. D1 and G peak parameters of samples from OriginPro. 70
Plate 15. D1 and G peak parameters of samples from OriginPro. 71
Plate 16. Histogram of the reflectance measurement of sample #1. 72
Plate 17. Histogram of the reflectance measurement of sample #2. 72
Plate 18. Histogram of the reflectance measurement of sample #3. 73
Plate 19. Histogram of the reflectance measurement of sample #4. 73

CHAPTER ONE

INTRODUCTION

The post-Covid-19 economic status and extensively stressed geopolitics of the world requires consolidation of energy supply resources. Even with the increased worldwide bias for rapid green-energy transition for a net-zero CO_2 future, increased energy demand and national economic needs of the countries urges the policy makers to select more conventional approaches for near-future planning for the energy supply chain. As a result, coal still stands as one of the most important energy items for developing countries. Türkiye is one of those countries with high fossil fuel usage and import dependencies (Erat et al., 2021) and needs to continue relying on coal, particularly lignite, as the most abundant energy resource. Hence, a detailed understanding of lignite deposits and their characteristics is needed for clear planning of the future mining strategies.

One of the prolifically used tools for understanding the coal characteristics today is organic petrography, and lately the micro-Raman spectrometry. Organic petrography has a variety of applications such as, determination of the coal rank, correlation of coal layers among boreholes, interpretation of geological structures in the coal-bearing sedimentary basins, reconstruction of the paleoenvironment, studies on diagenesis of sediments, exploration of geothermal fields and hydrocarbons, technological studies on coal blends etc. Recent studies increasingly try to focus on answering questions for environmental concepts and applications such as environmental forensics, environmental modelling and nature-based solutions for net-zero emissions. Although this environmental leg of organic petrography is somewhat new, the former conventional applications pronounced are largely adopted and applied in the coal producers.

Raman spectroscopy is a method used for determination of structural characteristics of the carbonaceous material since 1970s (Li et al., 2006, Azeri, 2023). In the 1970s, the designation of the Raman spectral bands has been largely discussed. Numerous articles on exploring the characteristic Raman scattering of carbon material (e.g., macerals in coal) have been published since then (Potgieter-Vermaak et. al., 2011).

Later studies also focused on inorganic and maceral character of coal and changes during coking (e.g. Green et al., 1983) and more recent research of the last two decades mainly concentrated on the applications regarding Raman-sensitive bands identified in 1970s to 1990s work (cf. Potgieter-Vermaak et al., 2011). Today, the method is mainly used to determine the thermal alteration (maturity) of organic matter and regarded as one of the many tools for understanding thermal maturity of the organic matter along with other techniques such as vitrinite reflectance (VRo), bitumen reflectance, graptolite reflectance, etc (Henry et al., 2019). Work on low-rank coal however is not wide-spread. Few papers have been published from lignite macerals (e.g., Bielowicz and Morga, 2021).

1.1. Aim of The Study

The objectives of the study mainly are to determine the petrographical, mineralogical and geochemical characteristics of the coal cored at borehole B-22 (randomly named and roughly located in the Figure 1 due to the company policy and permissions) within the Yatağan Thermal Power Plant. In order to do this, the above-mentioned petrographic and spectroscopic methodologies are applied to coal samples as well as the X-Ray based mineralogical and chemical work. Proximate and calorimetric analyses from earlier work of Erecek (2020) have been incorporated for complementary purposes. The aim is to provide a first idea on coal features, depositional environment and evolution of the coal in this greenfield.

1.2. The Study Area

The study area is a newly discovered coalfield located within the license boundaries of the Yatağan Thermal Power Plant, between Şahinler-Bozüyük in the southwest of Yatağan district of Muğla Province in southwestern Turkey (Fig. 1). The area is around 28 km away from Muğla and 79 km from Aydın; the location of the field is northwest of the Bayır Sector and southeast of the Turgut Sector.

Yatağan district and its surroundings have a Mediterranean climate. In the district, there is 75% red pine, 5% larch, and 1% pistachio pine. Secondary vegetation consists of thyme, blackberry, sycamore and poplar. Olive and tobacco cultivation are practiced throughout the region.

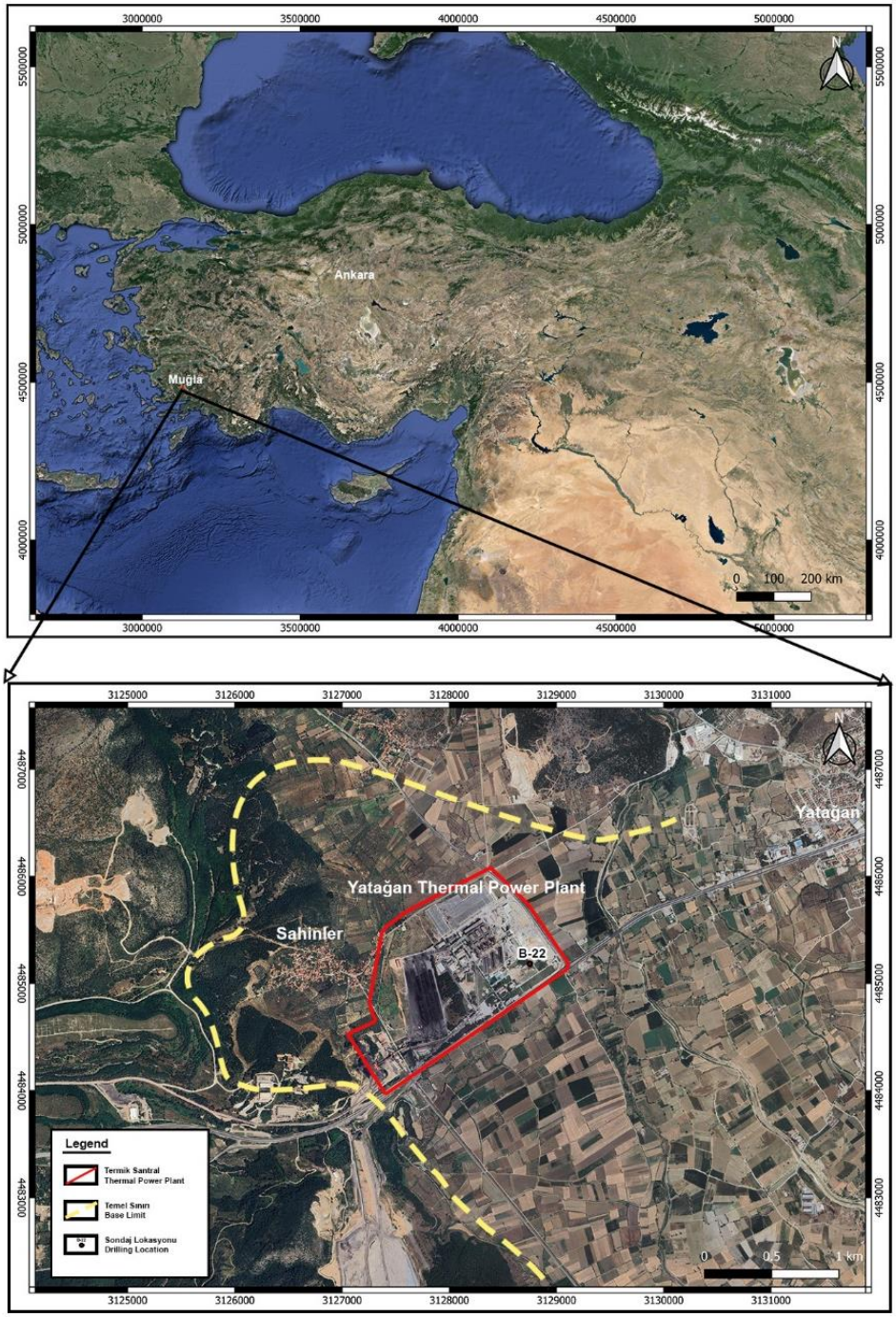

Figure 1. The location of the study area and the roughly located #B22 drillhole; the red line shows the boundary of the thermal powerplant, the dashed yellow line show the boundary of licence.

1.3. Previous Studies

The first prospecting campaign in the Yatağan area was carried out in 1965 by jointly the General Directorate of Mineral Research and Exploration (MTA) and the German Consulting Company OTTO GOLD. MTA started drilling activities in 1974 following the 1/25,000 and the 1/10,000 geological mapping studies, whereas the feasibility studies were completed in 1978. Between 1980 and 1990, operational works were initiated by the Turkish Coal Enterprises (TKİ).

As a result of the above prospecting studies carried out by OTTO GOLD in 1965, the company concluded that there are coal-bearing parts of Turgut Formation in Bağyaka but they are economically not feasible.

The stratigraphic sequence of the Eskihisar Sector of the Muğla lignite Neogene was described in the report prepared by Kasap and Ünal (1987). These authors report that the basement is composed of metamorphic schists of the Menderes Massif, the crystallized limestones are followed by Turgut and Sekköy Formations and the lignite horizon is located between these two Formations and alluvial deposits.

Kasap and Ünal (1989) report that eight (8) boreholes were carried out by MTA in the south of the Bağyaka Sector in order to determine the coal field boundary.

İnaner (1994) conducted determinations on chemical properties, reserve estimation and feasibility study of the lignite-bearing basins in Southwestern Anatolia.

Querol et al. (1999) conducted a joint project with the North Atlantic Treaty Organization (NATO) and MTA to determine the geological features and the coal quality in the Muğla Basin.

In 2010, MTA studied in detail the geology and the chemical properties and estimated the reserve quantities of the lignite deposits in Turkey and published a general report.

Büçkün (2013) conducted a master's thesis on the coal quality, mineralogical and maceral composition of the Miocene Hüsamlar lignite in the Muğla-Milas Basin.

Koç (2017) analyzed and palynologically evaluated the fossils in marlstones from the Tınaz Basin and Sekköy Formations.

Yakupoğlu (2017) studied the Neogene Muğla Basin and proposed the depositional environments using the sedimentological and petrographic properties of the sedimentary rocks.

Erecek (2020) has conducted a preliminary petrographic and proximate analytical work on the samples obtained from the subject drillhole cores during her bachelor's thesis. However, the petrographic leg of this study had been very limited and included very few details on the macerals.

Erecek et al. (2023) later studied the coal-petrography, mineralogical and geochemical characteristics on samples taken from the area in detail and published her preliminary findings of the current study.

Hacımustafaoğlu et al. (2023) measured the reflectance of various huminite macerals on lignite samples taken from the subject field and examined the relationship between them. The study concluded that the average reflectance values of ulminite B, corpohuminite and gelinite are quite similar, while values for ulminite A are substantially lower, noting a strong positive correlation between the average corpohuminite and gelinite values at $\alpha = 0.05$ significance level ($R^2 = 0.94$).

CHAPTER TWO

GEOLOGICAL SETTING

The geology and columnar section of the study area are given in Figures 2 and 3. The compiled data are from Gold (1965), Nakoman (1971, 1978, 1982), Ünal (1987, 1989), Nakoman and Inaner (1990) and Gürsoy et al. (1993). In summary, gneiss and schists constitute the basement rocks in the study area. The coal seam is hosted in-between the Miocene Turgut and Sekköy Formations, which include intercalations of claystone, siltstone and fossiliferous limestone. The younger Yatağan and Milet Formations overly these coal-bearing formations.

The Yatağan Basin is a NW-SE trending half-graben between Şahinler in the northwest and Salihpaşalar in the southeast (Fig. 2), bounded by the Yatağan normal fault on the southwestern edge, about 20 km long and up to 7 km wide. Yatağan Half Graben is located between the Büyük Menderes Graben to the north and the Gulf of Gökova to the south. The rock assemblages belonging to the Menderes Massif and tectonically overlying Lycian Nappes form the basement rocks. This crystalline and overlying allochthonous basement rocks are unconformably overlain by the cover series of varying ages ranging from Eocene to the present (Kürçer and Gürsoy, 2022).

2.1. Pre-Neogene Formations

Pre-Neogene formations are represented by the basement rocks outcropping to the margins of the Yatağan Basin and consist of Palaeozoic gneiss, schist, and Mesozoic marble. The basement rock consisting of schist, gneiss and recrystallized limestone are the oldest unit of the Muğla Basin (Fig. 3).

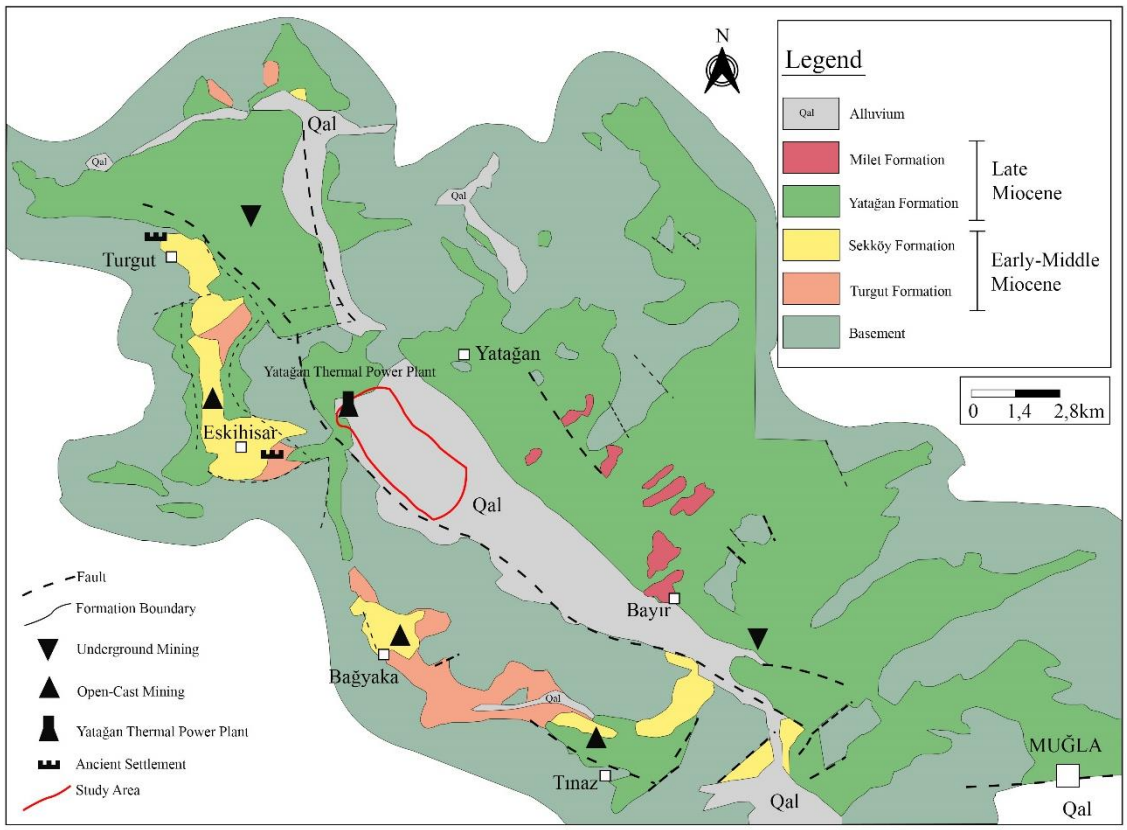

Figure 2. Geological map of Yatağan Basin (Ünal, 1989; Bulut et al., 2001).

2.2. Neogene Formations

2.2.1. Turgut Formation

Among the Neogene deposits outcropping in the region, the lowest is the Turgut Formation, which is around 200 m thick. The sediments underlying the main productive coal seam at the site consist of conglomerate, claystone, siltstone, sandstone and gravels. Where the basement is close to the depositional area, the formation consists of gravels, boulders, and abundant micaceous sand with variable scale cross-bedding, probably originating from unidirectional fluvial currents (Querol et al., 1999).

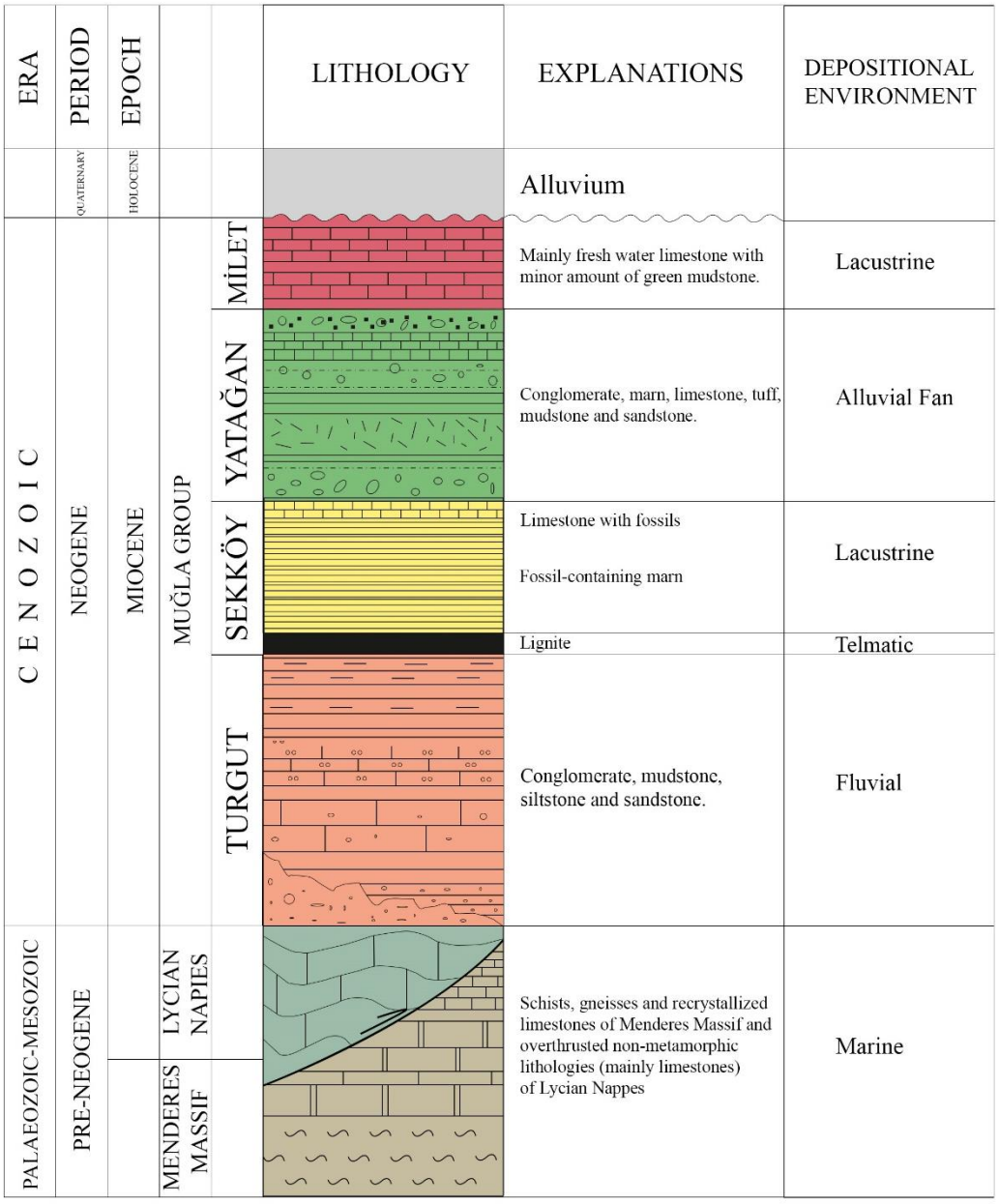

Figure 3. Generalized lithostratigraphic section of the Muğla-Yatağan lignite basin (after Gürsoy et al., 1993, İnaner, 1994).

2.2.2. Sekköy Formation

The Sekköy Formation is conformable with the Late Miocene aged Yatağan Formation above and the Early-Middle Miocene aged Turgut Formation beneath, and coal seams are found in the lower segment of the formation (Yiğitel, 1979). It overlies lignite layers ~20 m thick and is represented by a stack of grayish and olive green-coloured compact marlstone at the bottom and a laminated marlstone, thin limestone and claystone succession towards the top. This formation includes detrital facies consisting of limestone and conglomerate at the basin margins and transitional facies consisting of a sequence of poorly consolidated claystone and siltstone interbedded with the Yatağan Formation (Querol et al., 1999). The Formation environment of the Sekköy Formation is stated as a lake environment (Atalay, 1980).

2.2.3. Yatağan Formation

Yatağan Formation is Upper Miocene in age and its dominant lithology is reddish brown, medium- and coarse-grained sandstone ~600 m thick. The Sekköy Formation underlies the Yatağan Formation, whereas the Milet Formation conformably overlies (Fig. 3). The upper segment is generally represented by coarse-grained alluvial deposits and the lower segment by yellow sandstone and siltstone gradually covering the marlstone of the Sekkoy Formation. Mammalian fossils are abundant in the Yatağan Formation (Querol et al., 1999).

2.2.4. Milet Formation

At the lower boundary of the Milet Formation is the Yatağan Formation, to which it is conformable, and at the upper boundary is the unconformable Quaternary deposits, followed by a 1-2 m thick siltstone with lignite interlayers at the base (Querol et al.,

1999). The formation thickness is approximately 140 meters. Atalay (1980) has found gastropod and mammalian fossils in the marble and limestones and stated that the formation was a result of the uplift of lake environments.

2.3. Quaternary Formations

Quaternary deposits in the area consist of sand, clay and poorly graded pebble.

CHAPTER THREE

MATERIALS AND METHODS

Four core samples from B-22 borehole drilled within the Yatağan Thermal Power Plant site (Figs 1 and 4) has been provided by the company that conducted the exploration drilling. The borehole location and number could not be provided and presented here due to the company policy and the borehole number B-22 is given randomly. The samples were collected from depths between 570 and 580 m beneath surface. The cross section and location of the coal seam where the depths of the samples are located, are given in figure 5. As the samples were stored in the company's storage for long time, they had lost their moisture. After sampling, they were kept in plastic bags at $^{+}4^{o}C$ to minimize further moisture loss and oxidation.

The samples were properly prepared for proximate and petrographic analyses. Each sample was ground in agate mortar and passed through the 1 mm aperture sieve. The samples are then placed in an oven at 105ºC for 4 hours to remove the remaining moisture. Afterwards the samples were placed in a desiccator. The samples were then split into two parts for proximate and petrographic analyses.

The proximate analyses, determination of calorific values and the total sulphur content were performed in the Dokuz Eylül University, Department of Mining Engineering Chemistry Laboratory in 2020. Petri dishes, plunger dishes, quartz glass crucibles, porcelain crucibles and desiccators were used for the analysis. High temperature ovens were used for ash yield determination, IKA C200 calorimeter was used to determine calorific values and Eltra Elementary Analysis CS 2000 device was used for total sulfur content. Information on the analytical procedures are summarized in Erecek (2020) as follows.

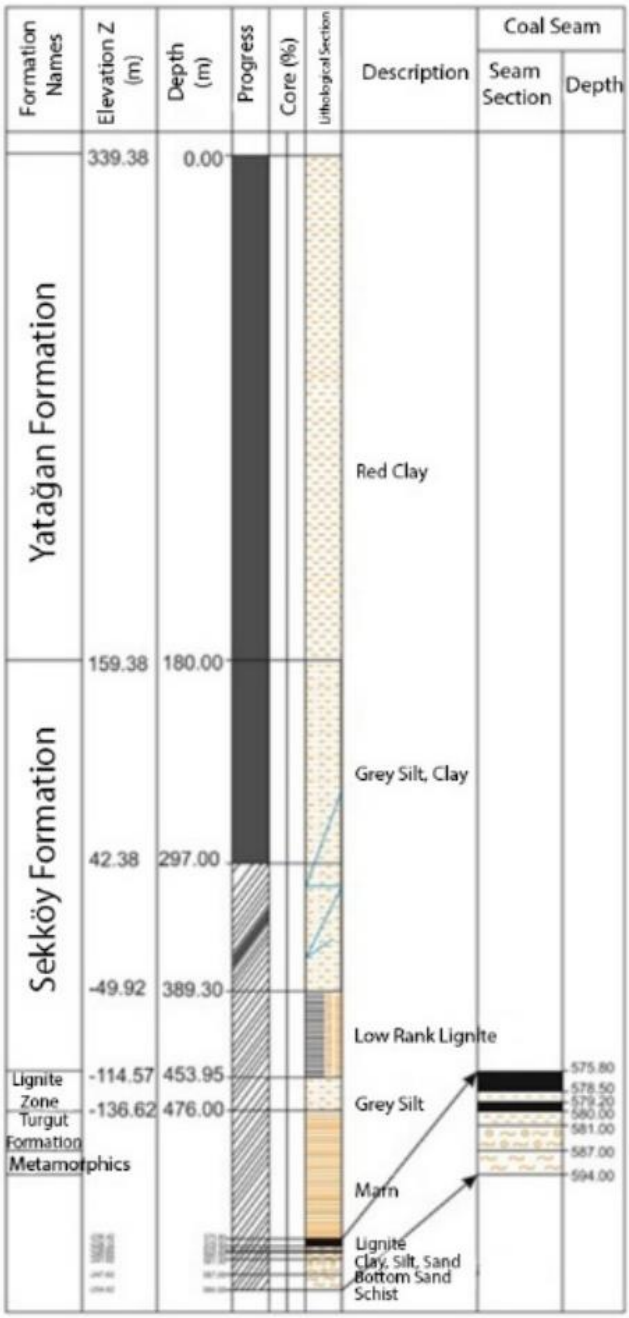

Figure 4. The lithostratigraphic section of the B-22 core with the sampling depths (Erecek, 2020).

Erecek (2020) reports that for the analyses of the ash yield, the empty (tare) porcelain crucible was placed in an oven at 800ºC for about 2 hours, removed and cooled, then weighed (Vk). Around 1 gram of sample was then placed in it, weighed again and noted ((N+V)k). Then, it was placed in an oven at 800ºC for about 4 hours. After removal and cooling, the sample was again weighed. The ash yield has then been calculated with the formula given below,

$$(FSk).Ash(\%) = FSk - Vk.[(N+V)k + 100]$$

where;

Vk = Empty weight of the porcelain crucible measured on a scale

(N+V)k = Empty porcelain crucible weight + total weight of the sample

FSk = Porcelain crucible removed from the oven + weight of the sample.

Only the total residual moisture remaining of the samples could be determined as the samples remain stored for very long time.

For volatile matter yield (VM) provided in this study, Erecek (2020) describes the procedure as follows: The samples were placed in an oven at 950ºC for 1 hour to reach a constant weight. After that, the quartz crucible containers were removed from the oven, cooled and weighed empty (tare) (Vum). After adding approximately 1 g of sample, ((N+V)um). After keeping the test containers containing the samples at 950ºC for about 6 minutes, they are removed, cooled and weighed again (FSum).

% Moisture + Volatile matter had been calculated with the formula written below,

$$\%(Moisture + Volatile) = (N+V)um - FSum(N+V)um - Vum$$

where;

Vum = Empty weight of the crucible container

(N+V)um = Weight of empty crucible and total weight of 1 g sample

FSum = Quartz crucible removed from the oven + weight of the sample.

The calculated % Moisture value is subtracted from the result obtained with the formula to obtain the % Volatile matter yield.

The following procedures are further summarized by Erecek (2020) for the calorific value measurements and total sulphur content. The calorimeter beaker was thoroughly cleaned with distilled water. The crucible was thoroughly dried after cleaning with distilled water. The sample was weighed to 0.4-0.5 g. O_2 (oxygen) was pressed at 30-32 bar for 45 seconds, the sample was sealed and placed in the measuring device, the sample was weighed and put into the device and the measurement was completed.

To determine the total sulphur value, 0.1 g sample was placed in the Eltra Elementary Analysis CS 2000 device, after being kept at 1350ºC for approximately 180 seconds, then it was removed and the results were read on the instrument computer.

Portable XRF-XRD analyses for this study were conducted by an OLYMPUS DELTA Premium DP-6000 portable X-ray fluorescence (PXRF) at Dokuz Eylül University Torbalı Vocational School (Fig. 5). X-ray diffraction (XRD) measurements were performed at the X-Ray Laboratory of Dokuz Eylül University Department of Geological Engineering via a Rigaku MiniFlex 600 diffractometer. The XRD measurements are completed on randomly oriented grains using CuKα radiation (k=1.542 Å). The analytical conditions were set as 33 kV and 15 mA, scanning 2-65° of 2θ with a step size of 2°/min. The crystalline phase identification was carried out using the PDXL2 software package (Rigaku).



Figure 5. OLYMPUS DELTA Premium DP-6000 (Portable-XRF Measuring Device).

For petrographic analyses, polished blocks of coal samples were prepared after grinding to Ø < 1 mm, in accordance to the ISO 7404-2 standard. They were prepared in the Organic Petrography Laboratory of Dokuz Eylül University, Department of Geological Engineering. Maceral analyses were also completed in the Organic Petrography Laboratory of Dokuz Eylül University Department of Geological Engineering. Polishing of the sections were performed using a Struers LaboForce-50 equipment. The maceral analysis was performed at maceral-group/sub-group level (ISO 7404-3) using a LEICA DM 4500 P microscope (Fig.6), in oil immersion, under incident white light and blue-light excitation. The microscope installed at the Organic Petrography Laboratory is equipped with the Hilgers FOSSIL MOT software. The maceral nomenclature applied is this of ICCP System 1994 (ICCP, 1991; Sýkorová et al, 2005; Pickel et al., 2017). Reflectance measurements were performed according to ISO 7404-5 on Ulminite B macerals. For the maceral analysis, a minimum of 500 points (in an area of ~4 cm^2) in each sample were determined. Reflectance was measured on a minimum of 150 points for each sample. The results of the maceral-group analysis are provided in volume percentage (vol%) for each of the four groups/sub-groups and in percentage (%) for the reflectance values.

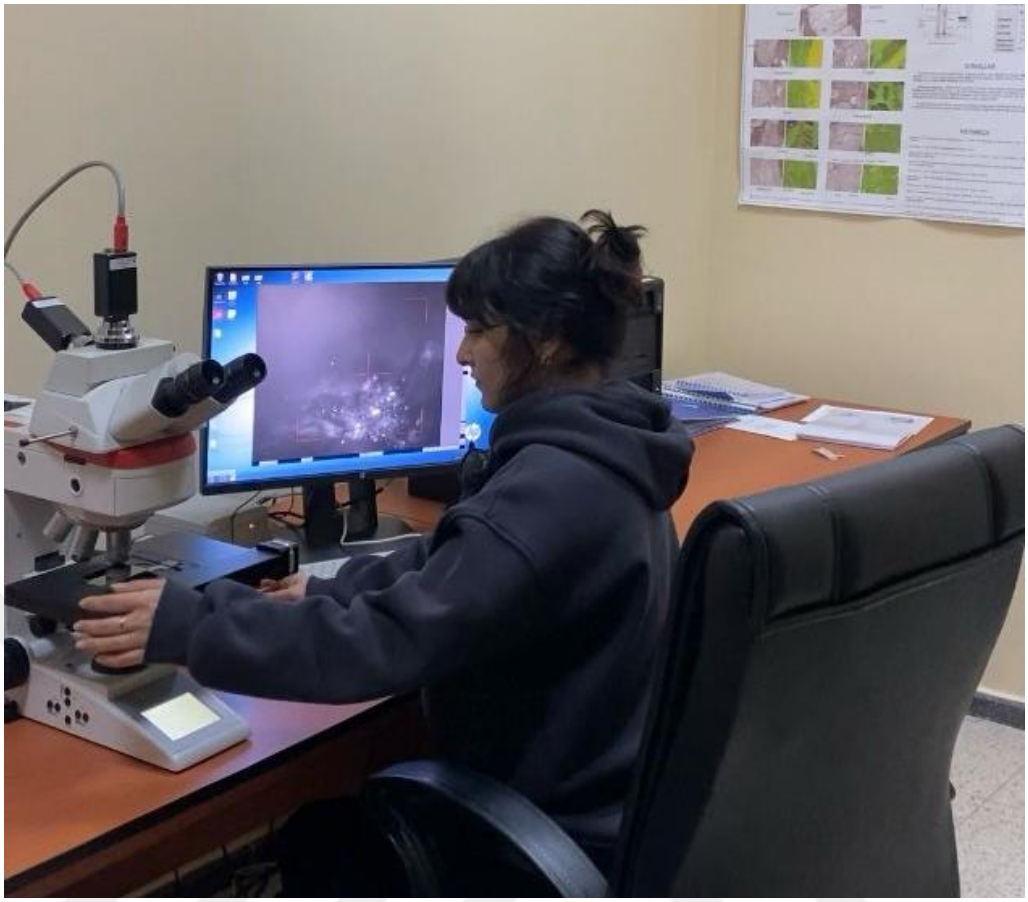

Figure 6. Maceral analysis of samples with LEICA DM 4500 P brand microscope.

The polished sections used for petrographic analyses were also used in micro-Raman spectroscopic study. Raman spectroscopy analysis was carried out using a Confocal Renishaw inVia Raman Microscope and Spectrometer installed at İzmir Katip Çelebi University Central Research Laboratories Application and Research Center (İKÇÜ-MERLAB). Raman measurements were performed after the maceral analysis and reflectance measurements were completed. The micro-Raman spectroscopy was performed on the selected fusinite and ulminite macerals. Initially it was planned to examine two samples from the borehole, however one sample was damaged (singed) due to initial high energy settings, thus the measurements were completed on one sample only.

The instrumentation used to perform the Raman measurements (Fig. 7) used a 100x magnification objective lens. The laser source was set as 532 nm, the available grating value was 2400 l/mm. The spectral range of the system varies from 260 cm^{-1} to 3300

cm^{-1}. The laser is applied superficially with a diameter of 26μm to the designated point on the bright section. The data obtained after the analyses, was processed using three different available spectroscopy software; SpectraGryph 1.2, OriginPro 2023 and the IFORS (with Python software) (Lünsdorf et al., 2017). The results were evaluated via crosschecking the data obtained from these three programs.



Figure 7. View of the Renishaw Raman Spectroscopy instrument.

CHAPTER FOUR

RESULTS

4.1. Definitions of the Studied Macerals and Maceral Subgroups and Huminite Reflectance Measurements

The term maceral is firstly introduced by Stopes (1935) to define the organic building components of coal recognizable under the microscope as an analogy to the minerals.

Spackman (1958) has later improved the definition by Stopes (1935) stating that; "*... macerals are organic substances or optically homogeneous aggregates of organic substances that have distinctive physical and chemical properties and occur naturally in sedimentary, metamorphic and igneous materials of the earth.*"

Macerals are classified into 3 groups: vitrinite/huminite, liptinite and inertinite (ICCP, 1994).

4.1.1. Vitrinite/Huminite

According to Sýkorová et al. 2005, huminite and vitrinite maceral groups are associated for the parallel use of the two systems. Huminite group macerals are lignite (soft brown coal) counterparts of the vitrinite macerals in hard coal. During the progressing coalification, the cellulose of the terrestrial plant remains goes through humification to firstly form huminite and at further coalification levels to vitrinite, while the lignin goes through fusinitisation to form inertinite. Resin and waxes of the plant remains that are relatively resistant against fusinitisation form the liptinite macerals (Fig. 8).

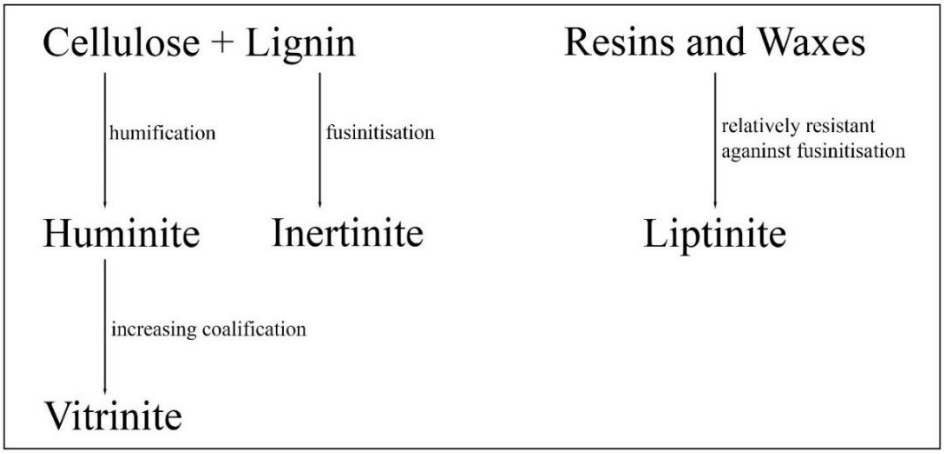

Figure 8. Simplified pathways of maceral genesis (ICCP course Organic Petrology notes, 2022).

Huminite consists of the cell filling material belonging to the tissue that forms the roots, stems, branches and bark of plants (Ünalan, 2010). Huminite is distinguished into 3 subgroups, namely telohuminite, detrohuminite and gelohuminite. Short descriptions of these subgroups are given in Table 1.

Table 1. Huminite group macerals (modified from Ward, 1984).

Maceral Group	Maceral Sub-Group	Maceral	Description
HUMINITE	Telohuminite	Textinite	Cell walls either of isolated-but intact individual-cells or within tissues
		Ulminite	Cell filling; partly or fully gelified tissues
	Detrohuminite	Attrinite	Mixture of fine non-gelified amorphous huminite particles (<10μm) of various shape
		Densinite	Mixture of fine huminite particles (<10μm) of various shape cemented by amorphous dense huminitic (gel) substance
	Gelohuminite	Gelinite	Homogeneous and structureless infillings of cracks and other voids
		Corpohuminite	Homogeneous and discrete bodies representing cell infillings

4.1.2. Liptinite

Liptinite group macerals mainly originate from hydrogen-rich parts of plants such as spores, pollen, cuticle, resin and blue-green algae (Ünalan, 2010). However, in 1989, Teichmüller has realized that liptinite is also derived from decomposition products as well as the hydrogen-rich plant organs, a finding that is important for the chemistry, understanding and interpretation of liptinite macerals. Liptinite group macerals are easily distinguished from other maceral groups with their fluorescence feature under blue or ultraviolet excitation. Short descriptions of liptinite group macerals are summarized in Table 2.

Table 2. Liptinite group macerals (modified from Ward, 1984).

Maceral Group	Maceral	Description
LIPTINITE	Cutinite	Constituent formed from cuticles of leaves and stems
	Suberinite	Cell walls filled with corpohuminite which differ from humotelinite by virtue of their liptinitic character and are derived from suberized cell walls
	Sporinite	Outer cell walls of plant spores and polen
	Resinite	Discrete bodies of varying shape (round, oval, rod-like) or diffuse impregnations; it can also fill in cell lumens of textinite/telinite; fluorinite displays greenish fluorescence colour
	Liptodetrinite	Small particles of liptinite macerals; can no longer be assigned with certainty to one or other maceral of the liptinite group
	Chlorophyllinite	Particles with characteristic blood-red fluorescence; after short time of irradiation red colour disappears
	Bituminite	Fine-granular ground mass or laminae, irregular streaks, wisps, podsi bands and elongated lenses with vein-like apperarance, fine disseminations as seen in perpendicular sections or as more homogenous, diffuse, equidimensional particles of various shapes in horizontal sections
	Exsudatinite	Secondary maceral generated during coalification and intruding into empty spaces such as fissures, cracks and other cavities

4.1.3 Inertinite

The term inertinite was first coined by Teichmüller in 1989 to refer to the behavior of the maceral in coking-grade coals where it was thought that the maceral did not soften during carbonization. Teichmüller (1989) also added that the characteristics of inertinite macerals include high reflectance, low fluorescence, high carbon and low hydrogen content and strong aromatization (Scott, 2002). Inertinite group macerals originate from the trunk, branches, roots of large plants such as vitrinite and fungi. Ünalan (2010) described inertinite as partially burned and charred plant remains due to the effect of heat, or plant remains that have been excessively oxidized by the oxygen of the air in sometimes or seasonally dry mires. Short descriptions of inertinite macerals are given in Table 3.

Table 3. Inertinite group macerals (modified from Ward, 1984).

Maceral Group	Maceral	Description
INERTINITE	Fusinite	Well preserved cellular structure of at least one complete cell of parenchyma or sclerenchyma
	Semifusinite	Displays intermediate reflectance and structure between telohuminite/vitrinite and fusinite in the same sample
	Funginite	Single or multi-celled fungal spores, sclerotia, hyphae and mycellia (stomata, mycorrhiza) and other fungal remains
	Secretinite	Commonly round, vesicled to non-vesicled, equant to elongate bodies without obvious plant structure
	Macrinite	Amorphous matrix or discrete, structureless bodies of variable shapes which are commonly elongated when viewed perpendicular to bedding
	Micrinite	Very small rounded grains occurring close to liptinite macerals
	Inertodetrinite	Discrete small inertinite fragments of varying shape can no longer be assigned with certainty to one or other maceral of the inertinite group

Inertinite is formed as a result of the charring of some plant parts; the appearance, colour, H/C O/C ratios, densities, fluorescence properties and light reflecting ability (reflectance) of each of them under the microscope vary. Under incident light, huminite is observed as medium to light gray in colour, depending on the degree of coalification. It shows little or no fluorescence under ultraviolet excitation. Liptinite appears dark gray under the microscope and fluoresces yellow under blue or ultraviolet incident light. Finally, inertinite is observed as light gray-white under incident light, its reflectance is higher than this of other maceral groups, and it has no fluorescence feature (Ünalan, 2010).

4.2 Analytical Data from Borehole B-22: The Maceral Composition and The Reflectance

According to the results of the maceral analysis completed from B-22 samples, huminite group is the most commonly found maceral group on a whole rock basis (Table 4). In all samples, detrohuminite maceral is more common than gelohuminite and telohuminite maceral. Liptinite and inertinite group macerals are observed at approximately the same rate, ranging between 3-10% and 3-8%, respectively. The mineral matter content of the samples varies greatly between 3-41%, and mainly consists of framboidal pyrites. Maceral photomicrographs are presented in Appendix I.

Table 4. Group/sub-group analysis results of macerals.

Sample No	***22_1***	***22_2***	***22_3***	***22_4***
in vol.%, on whole rock basis				
Huminite	**89**	**63**	**78**	**47**
Telohuminite	15	16	13	8
Detrohuminite	53	42	57	31
Gelohuminite	21	5	8	8
Liptinite	**4**	**10**	**3**	**4**
Inertinite	**4**	**3**	**4**	**8**
Mineral Matter	**3**	**24**	**15**	**41**
Total	**100**	**100**	**100**	**100**
in vol.%, on mineral matter-free basis				
Huminite	**91.8**	**82.9**	**91.8**	**79.7**
Telohuminite	15.5	21.1	15.3	13.6
Detrohuminite	54.6	55.3	67.1	52.5
Gelohuminite	21.6	6.6	9.4	13.6
Liptinite	**4.1**	**13.2**	**3.5**	**6.8**
Inertinite	**4.1**	**3.9**	**4.7**	**13.6**
Total	**100**	**100**	**100**	**100**
Reflectance (%)	**0.29**	**0.23**	**0.23**	**0.25**
StDev (%)	0.20	0.18	0.22	0.12
N	500	648	500	500

Projecting the results of the reflectance, volatile matter (daf) and fixed carbon (daf) on the German and North American classification schemes, the samples fall in the range of peat and lignite coal, but much closer to lignite. According to the calorific value, all the samples are classified as lignite. Sample number 4 is not coal due to its high ash value and therefore, is not included in these averages. (Fig. 9).

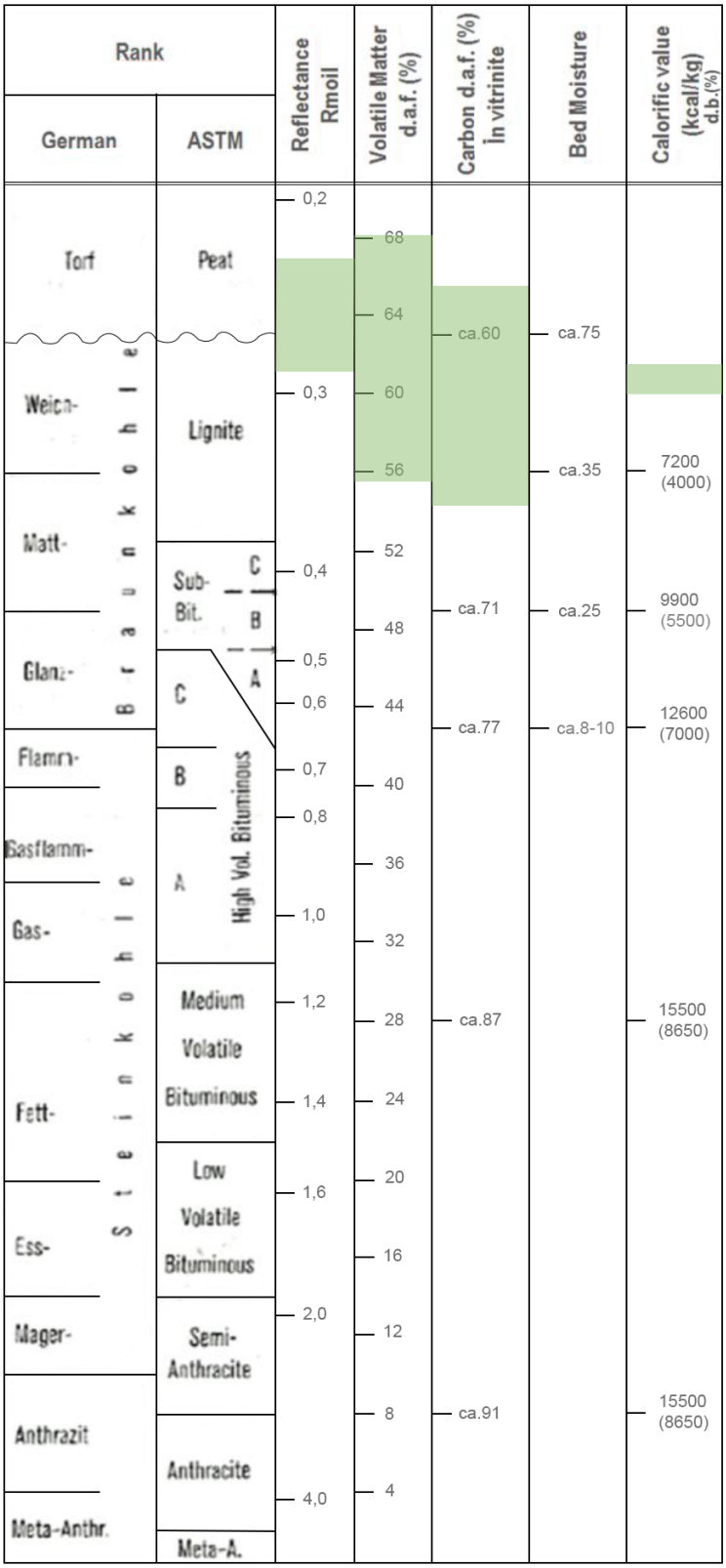

Figure 9. Rank determinations of studied coal samples in accordance to the German and North American classifications (after Taylor et al., 1998). Transparent greenfields denotes the ranges obtained and compiled from the coal samples.

According to the ECE-UN in seam Coal Classification (1998), Yatağan coal samples are classified as a medium-rank coal D, sample number 4 is carbonaceous rock (Fig. 10).

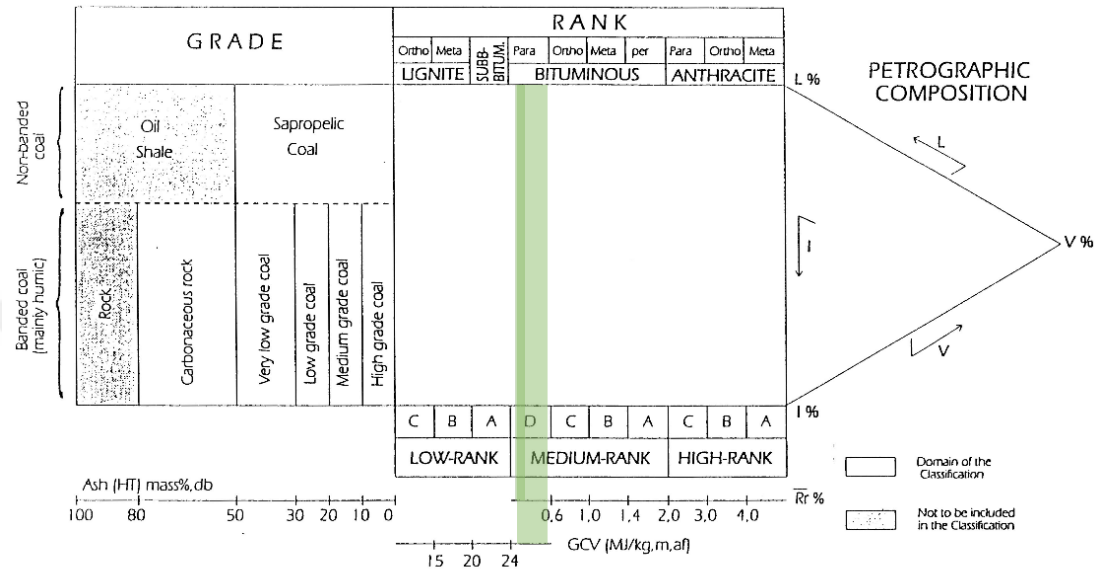

NB: Both designations of rank divisions (Low–Rank, Medium–Rank, High–Rank on one hand, Lignite, Sub–bituminous, Bituminous, Anthracite, on the other hand) apply to humic coals and to sapropelic coals as well.

$\bar{R}r$ % – Vitrinite Mean Random Reflectance, per cent (ISO 7404–5 Standard)
GCV (MJ/kg, m, af) – Gross Calorific Value in MJ/kg, recalculated to moist, ash free basis (ISO 1928 and 1170 standards), moisture being Bed Moisture , i.e. Total Moisture (ISO 1015 or 5068 standards)
Ash (HT) mass%, db – Ash content (High Temperature), mass per cent, recalculated to dry basis (ISO 1171, 331 and 1170 standards)
V%, L%, I% – Vitrinite, Liptinite and Inertinite contents respectively, volume per cent, mineral matter free (IS… 7404–3 Standard).

Figure 10. Coal rank determination according to the ECE-UN (1998) scheme. Transparent greenfield denotes spread of the samples.

The ABC ternary diagram proposed by Mukhopadhyay (1989) given in figure 12 shows a look on the dominant vegetation type and the oxic/anoxic conditions in the palaeomire prevailing during peat accumulation (Büçkün, 2013).

When the samples are illustrated in the ternary diagram (again, sample 4 was not included), they fall at the bottom right of the diagram and present anoxic environments with relatively high maceration and bacterial activity with increased reed-swamp vegetation. (Fig. 11).

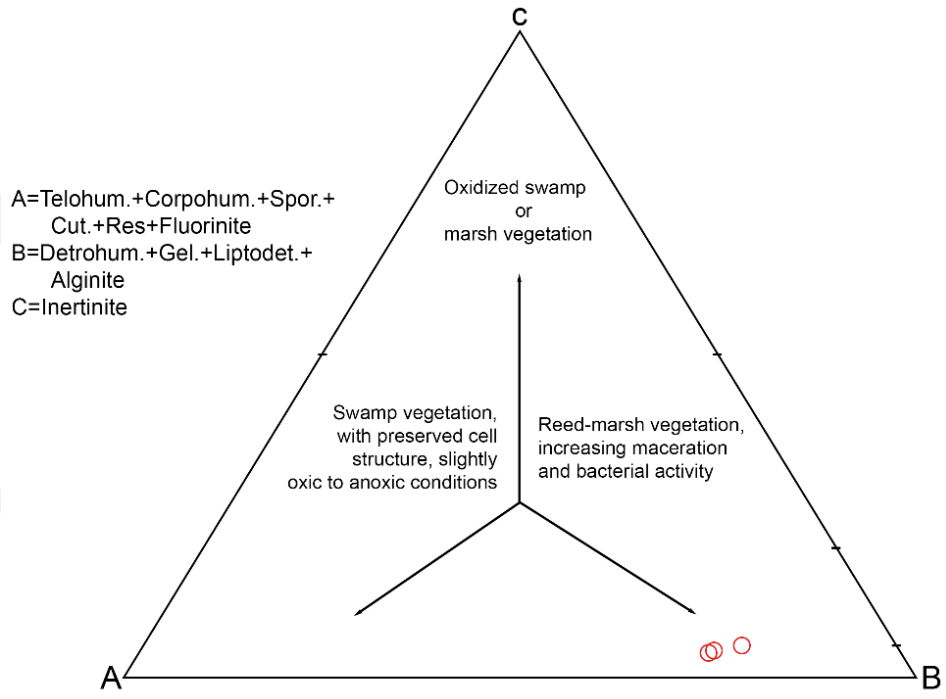

Figure 11. The ABC ternary plot of the Yatağan coal samples (after Mukhopadhyay, 1989).

4.3. Data from the Proximate Analysis

Proximate analysis provides direct information in determining the quality of coals and the properties and values of coal for commercial and other purposes (Toprak, 1996). As well as the organic petrographic work, throughout classification of the coal prerequisites the determinations of moisture, volatile matter and ash yields, calorific value, and the total sulfur content. Hence, the proximate analysis completed earlier by Erecek (2020) are re-evaluated here.

The moisture values of the samples were calculated on as-received basis, resulting in an average of 5.27%. Sample #4 was not included in the calculation of the average. That's done due to the high ash yield of the samples. The ash value of sample #4 is 71.50%, and according to ICCP 1994 it cannot be classified as coal, so it is classified as carbonaceous rock. In contrast, the average ash value of the other 3 samples is 35.38%.

4.4. Portable X-Ray Fluorecence (PXRF) and X-Ray Diffractometer (XRD) Results

Although being relatively a new field method, and somewhat problematic in some element sets, PXRF instrumentation is increasingly being used in initial evaluation of elemental abundances from unprepared field and core samples. PXRF measurements are performed on two of the samples. The samples with high ash content are selected in order to see the elemental variations. The data shows that the elemental abundances are 11.75-28.82% for Ca, 7.22-18.00% for Si, 0.12-2.6% for Al, 1.79-4.4% for Fe, 1.63-2.44% for Mg and 0.69-2.02% for K by weight (Table 5).

XRD spectrum obtained from the sample determined as a carbonaceous rock (sample 4) has revealed that the presence of mica, quartz, clay (chlorite/kaolinite/smectite), plagioclase, and calcite minerals (Fig. 12). An additional unknown peak is loosely considered as basaluminite (Felsőbányaite) [$Al_4(SO_4)(OH)_{10}\bullet_5 4H_2O$], which is regarded as a weathering product of clay minerals or iron-sulfide phases (pyrite/marcasite) phases.

Table 5. Elemental content of the samples obtained by PXRF spectrometer.

	Sample 3	**Sample 4**
Ca (%)	28.82	11.75
Si (%)	7.22	18
Al (%)	2.6	0.12
Fe (%)	1.79	4.4
Mg (%)	1.63	2.44
K (%)	0.69	2.02
Ti (ppm)	0.15	0.24
Sr (ppm)	660	240
V (ppm)	210	480
Mn (ppm)	350	112
Cr (ppm)	60	15
Zr (ppm)	40	110
Ni (ppm)	40	60
Zn (ppm)	30	110
Rb (ppm)	30	80
Ta (ppm)	26	50
Mo (ppm)	-	20
Nb (ppm)	12	160
As (ppm)	11	10
Y (ppm)	12	40
Hg (ppm)	5	-
P (ppm)	87	-

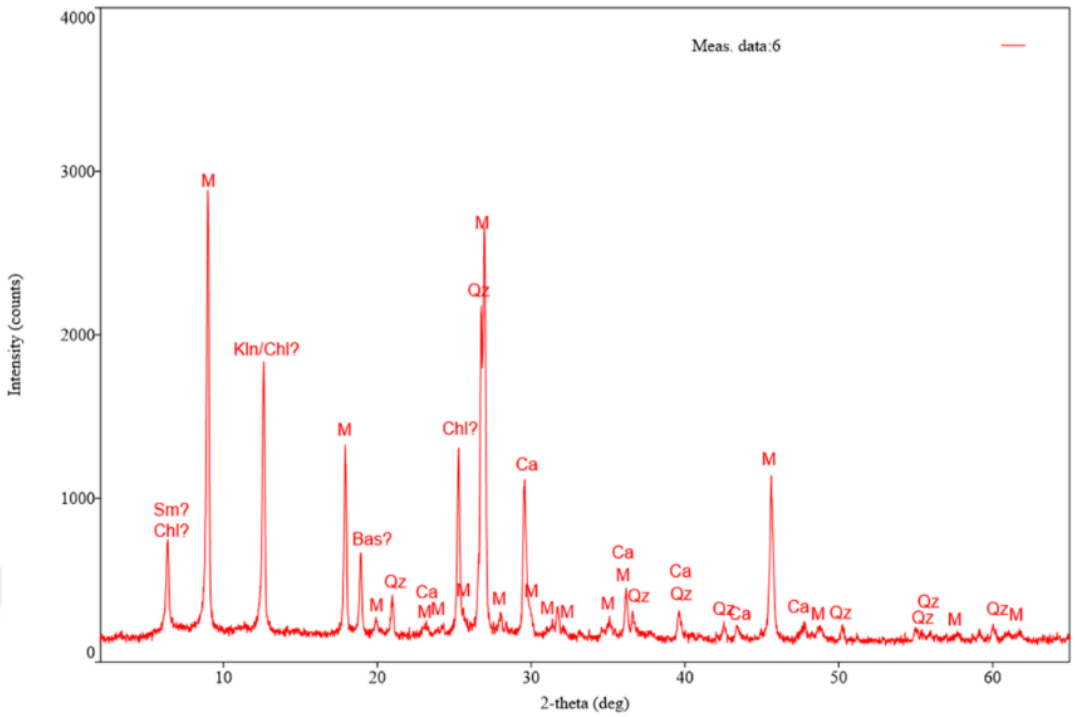

Figure 12. XRD spectrum of the sample 3 Abbreviations denotes,Qz: quartz, M: mica, Kln: kaolinite, Chl:chlorite, Sm: Smectite, Ca: calcite, Kfs: potassium feldspar, Pl: plagioclase, Bass: Basaluminite (Felsőbányaite).

4.5. Micro-Raman Spectroscopy

Raman scattering is caused by the inelastic scattering of bound atoms in the molecule or crystal lattice, which are exposed to a powerful laser source on the bright sections used in Raman spectroscopy measurement. By analysing the peaks in the spectrum obtained from these scattering, information about the functional groups which make up the structure of the material, can be obtained as well as qualitative and quantitative analysis of the material by looking at the bond structures of organic or inorganic substances in the sample.

Raman spectroscopy has been used extensively since 1970 to determine the structural properties of mostly carbonaceous matter (Li et al., 2006) and the thermal alteration (maturity) of organic matter (OM) (Henry et al., 2019a). It is a rapid and non-destructive method that can be utilized complementarily or independently, to study the samples prior to more expensive and destructive analyses (Sauerer et al., 2017; Schmidt et al., 2017; Henry et al., 2018, 2019b; Khatibi et al., 2018; Schito and Corrado, 2018; Wilkins et al., 2018; Henry et al., 2019a).

The determination of D (disordered) and G (graphitic) bands of the Raman spectra of the coal macerals has been a long-studied topic. Tuinstra and Koenig (1970) and Friedel and Carlson (1971) have firstly reported two broad bands in the 1355–1380 and 1575–1620 cm^{-1} regions of their analysed coal spectra and referred these bands as D (disordered) and G (graphitic) bands (Potgieter-Vermaak et al., 2011). Zerda et al. (1981) later reported widening of both the G and D bands in the low rank coals, noting lack of prominent relationship between the coal rank and G and D peak positions. Later work further focused on the selection of correct approach for deconvolution of the maceral Raman spectra (Potgieter-Vermaak et al., 2011). Other than the positions of the bands, several other Raman parameters are also compiled (e.g., full width at half maximum-FWHM, band intensities and areas, spectral ratios etc.) and used to evaluate the spectral characteristics of the macerals (Fig. 13).

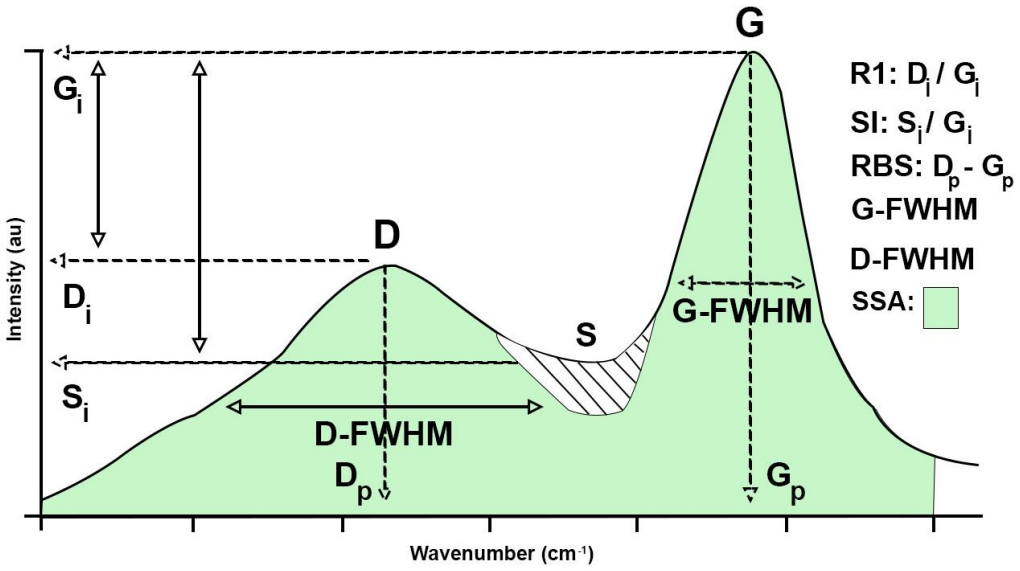

Figure 13. Example of Raman parameters and non-deconvoluted spectrum; Parameters of interest described here are saddle index (SI), Raman band separation (RBS), G-band/function full-width at half-maximum (G-FWHM), D band/function full-width at half-maximum (D-FWHM), scaled spectrum area (SSA) (Henry et al., 2019).

4.5.1. Micro-Raman Spectroscopy Data

In this study micro-Raman spectroscopy study has been completed on a single sample (sample #1). 14 points from 12 fusinite and 2 ulminite macerals are measured (Figs. 14-19 and Plates in Appendix II). The reason for the low number of ulminite data is mainly due to the hardship of detecting ulminite macerals under Raman microscope. Fusinite, on the contrary, is easier targets to detect. Ulminite maceral displays a stronger gelification and is therefore abundant in small aromatic units. However, it is harder to determine under Raman microscope than the fusinite. Fusinite is composed of larger, more various aromatic systems when compared to the huminite group of macerals and present a significant morphology, so it is easier to find it in the samples.

Gaussian-Lorentzian curve fitting method has been applied to obtain the data of the curves in the deconvolution of the Raman spectra. The parameter results calculated for

fusinite and ulminite macerals from the deconvolutions of the raw spectra were obtained via IFORS (Python based software), SpectraGryph and OriginPro programs. By peak deconvolution processes using these three programs, the D and G peaks for analysed macerals and Raman parameters are determined. The parameters obtained are given in Table 6.

According to these results, the values of the D1 bands peak positions of the fusinite macerals vary between 1345 and 1397 cm^{-1} with an average of 1375.17 cm^{-1}. The values of the D1 bands peak positions of ulminite are in the range of 1356-1362 cm^{-1} and average 1359 cm^{-1}. The values of the G bands peak positions in fusinite are in the range of 1587-1609 cm^{-1} and average 1598.75 cm^{-1}. The values of the G bands peak positions in ulminite are in the range of 1593-1594 cm^{-1} and their average is 1593.5 cm^{-1}. The average ranges of the D1 and G band positions obtained are within the range of values of the coal spectrum obtained from Tuinstra and Koenig (1970), and Friedel and Carlson (1971). The average width half height (FWHM) of the G bands peak positions in fusinites is 180.17 cm^{-1}, while the average width half height in ulminites is 214.50 cm^{-1}. While the width half height of the D1 bands peak positions for fusinite is 122.08 cm^{-1}, on average, it is 214.50 cm^{-1}, for ulminites.

The intensities of the unprocessed and deconvoluted Raman spectra show that the D- and G-band peak values of fusinite are lower than that of the ulminite. On the contrary, D- and G-band peaks are more pronounced in fusinite than in ulminite (Figs. 14-19).

Table 6. Raman parameters from the analytical data obtained via deconvolution of the curves of micro-Raman spectra (Abbreviations FWHM=Width at half height of the peak (cm^{-1})).

Sample ID	Maceral	Reflectance	D1 Bands Peak Positions (cm^{-1})	D1 Intensity	Left Point	Right Point	D1 FWHM (cm^{-1})	Area D1	G Bands Peak Positions (cm^{-1})	G Intensity	Left Point	Right Point	G FWHM (cm^{-1})	Area G	G-D1 (cm^{-1})	Area D1/Area G (AD1/AG)	Intensity D1/Intensity G (ID1/IG)
22_1_8	Fusinite	0.48	1382	15561	1323	1423	100	4549	1609	17741	1500	1677	177	2253	227	2.02	0.88
22_1_8_1	Fusinite	0.33	1397	8721	1332	1422	90	2315	1594	1014	1504	1654	150	1433	197	1.62	8.60
22_1_8_2	Fusinite	0.39	1381	8225	1325	1450	125	2978	1596	9826	1517	1677	160	1918	215	1.55	0.84
22_1_10	Fusinite	0.33	1377	10418	1330	1410	80	2608	1595	12088	1479	1667	188	2366	218	1.10	0.86
22_1_10_1	Fusinite	0.42	1381	14468	1324	1434	110	3915	1605	17037	1506	1678	172	2454	224	1.60	0.85
22_1_12	Fusinite	0.48	1368	12885	1324	1424	100	4649	1601	14568	1495	1685	190	2203	233	2.11	0.88
22_1_12_1	Fusinite	0.49	1375	8062	1319	1436	117	2129	1587	9326	1505	1653	148	1017	212	2.09	0.86
22_1_13	Ulminite	0.34	1356	2712	1225	1460	235	1423	1593	32552	1471	1696	225	3005	237	0.47	0.08
22_1_13_1	Ulminite	0.37	1362	2668	1286	1415	129	5537	1594	31672	1471	1675	204	2916	232	1.90	0.08
22_1_13_2	Fusinite	0.42	1345	2468	1243	1483	240	1336	1596	29339	1495	1670	175	2501	251	0.53	0.08
22_1_14	Fusinite	0.30	1373	10105	1312	1432	120	544	1599	11853	1508	1680	172	2255	226	0.24	0.85
22_1_16	Fusinite	0.42	1378	10754	1310	1430	120	5013	1605	12876	1476	1701	225	2926	227	1.71	0.84
22_1_19	Fusinite	0.40	1374	17562	1299	1452	153	8663	1597	19957	1480	1700	220	293	223	29.57	0.88
22_1_19_1	Fusinite	0.42	1371	21125	1305	1415	110	6481	1601	23721	1490	1675	185	2457	230	2.64	0.89

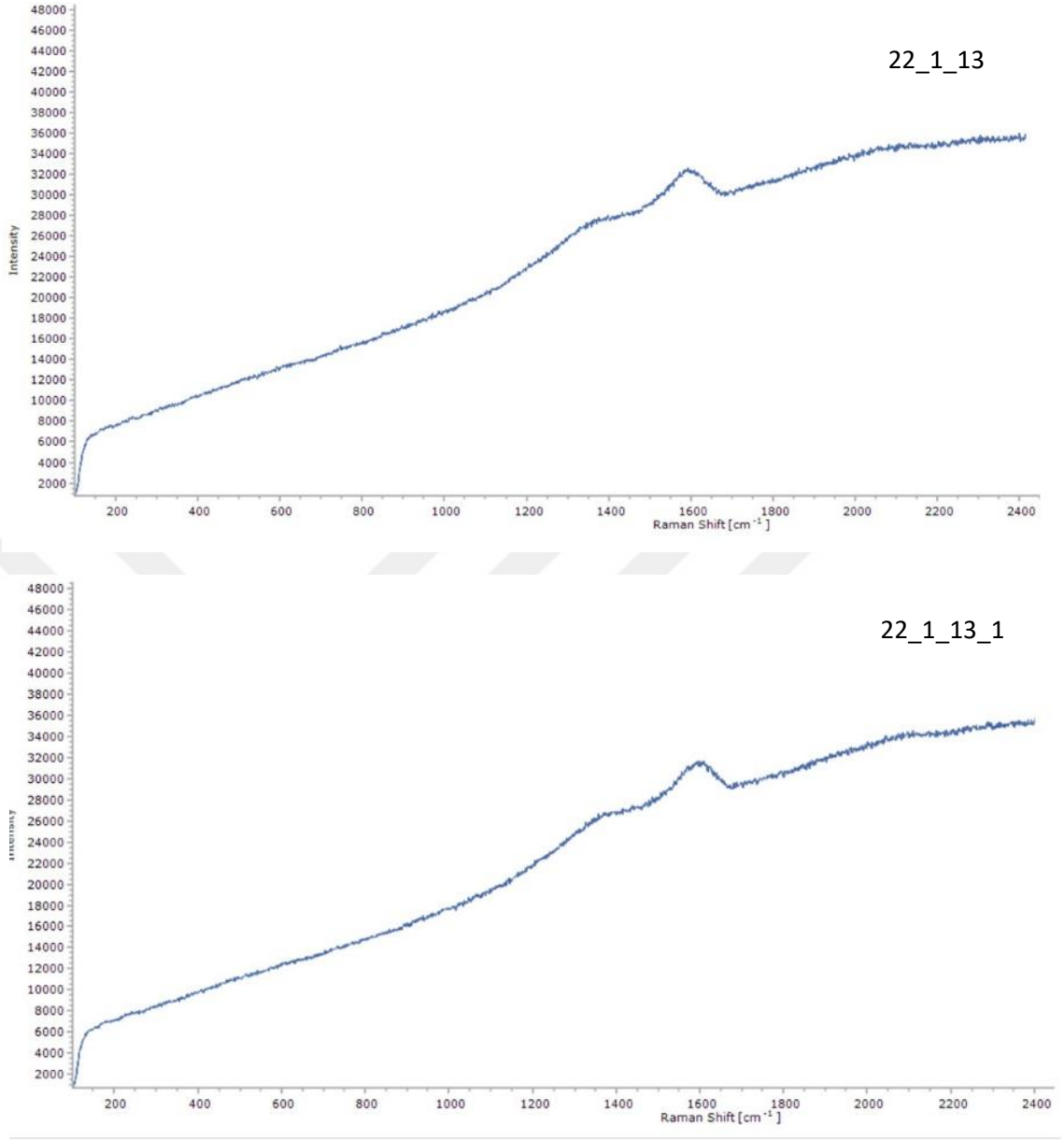

Figure 14. Examples of unprocessed visuals of the D- and G-band curves of 22_1_13 and 22_1_13_1 ulminite maceral. Visuals are illustrated via SpectraGryph software.

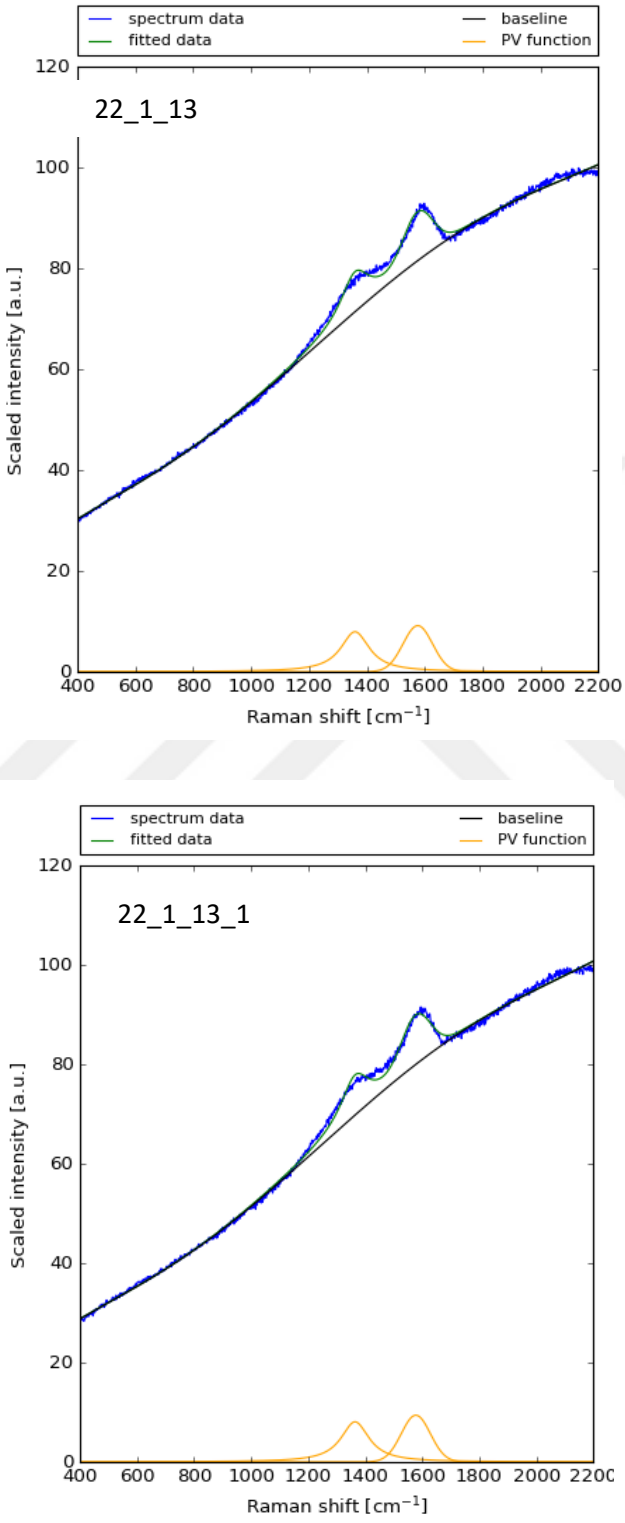

Figure 15. Examples of the D- and G-band curves of 22_1_13 and 22_1_13_1 ulminite maceral. Deconvolution curves and visuals are illustratedusing Python based IFORS software.

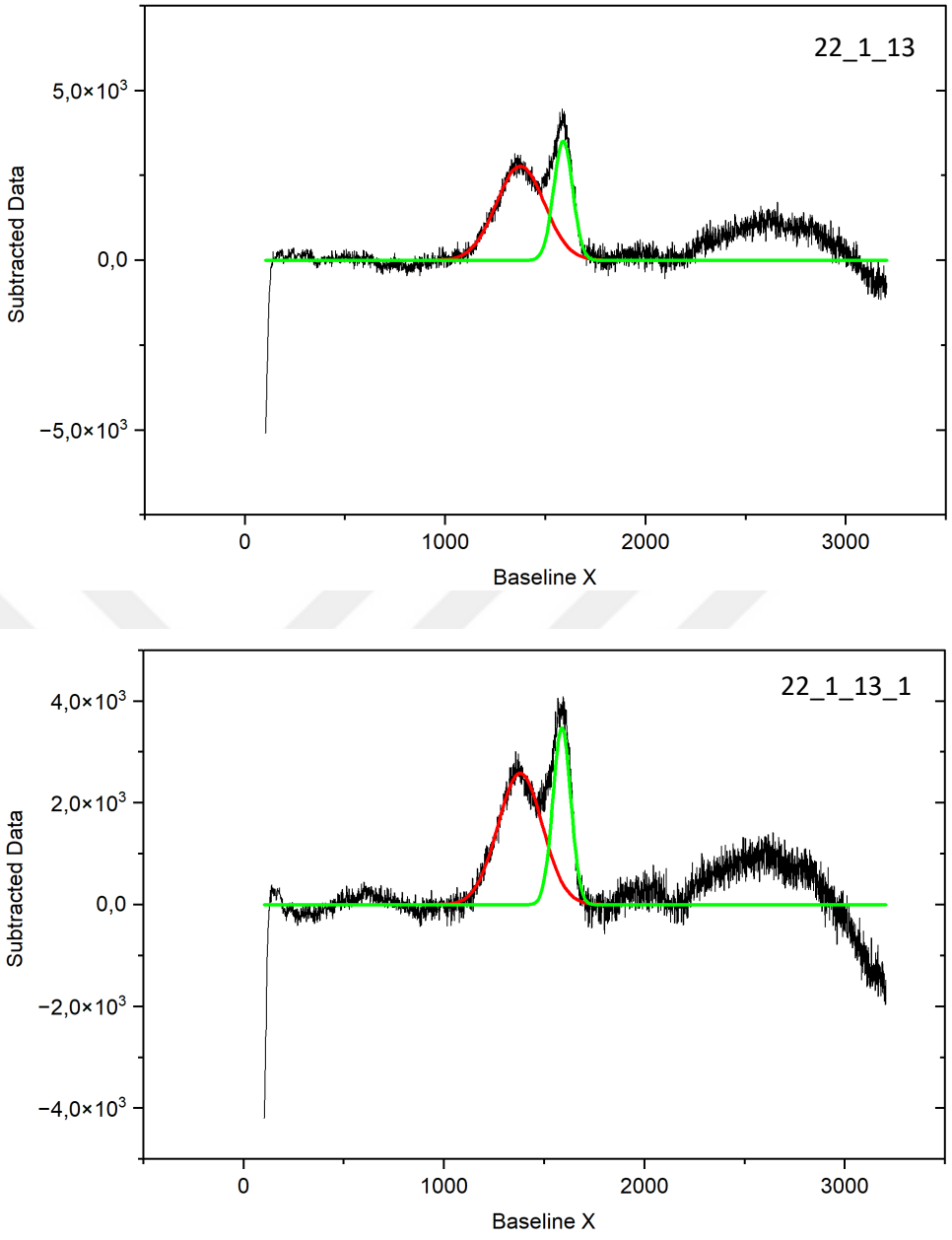

Figure 16. Examples of the D- and G-band curves of 22_1_13 and 22_1_13_1 ulminite maceral. Deconvolution curves and visuals are illustrated via generated using the OriginPro software.

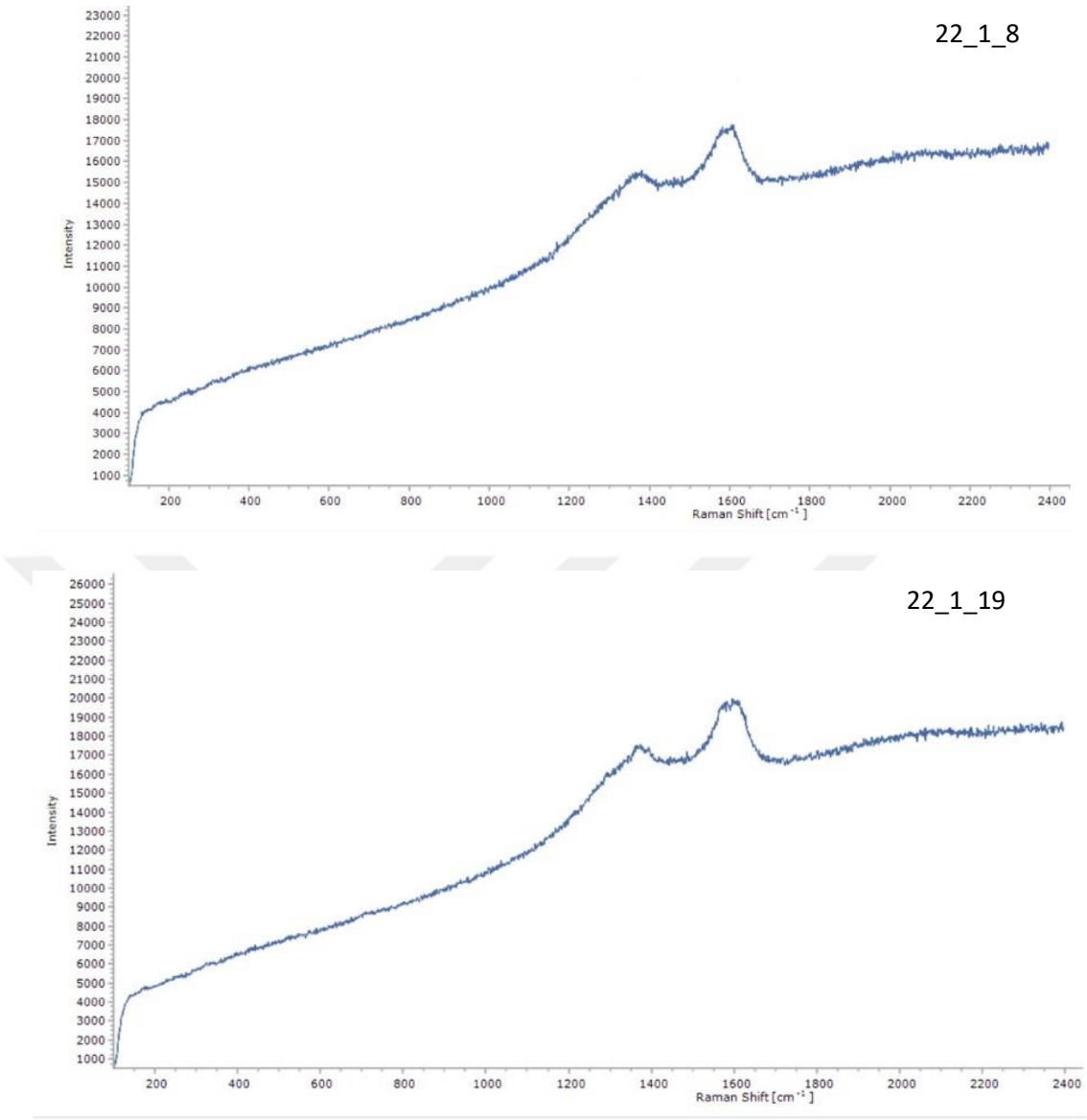

Figure 17. Examples of unprocessed D- and G-band curves of 22_1_8 and 22_1_19 fusinite maceral. Visuals are from SpectraGryph software.

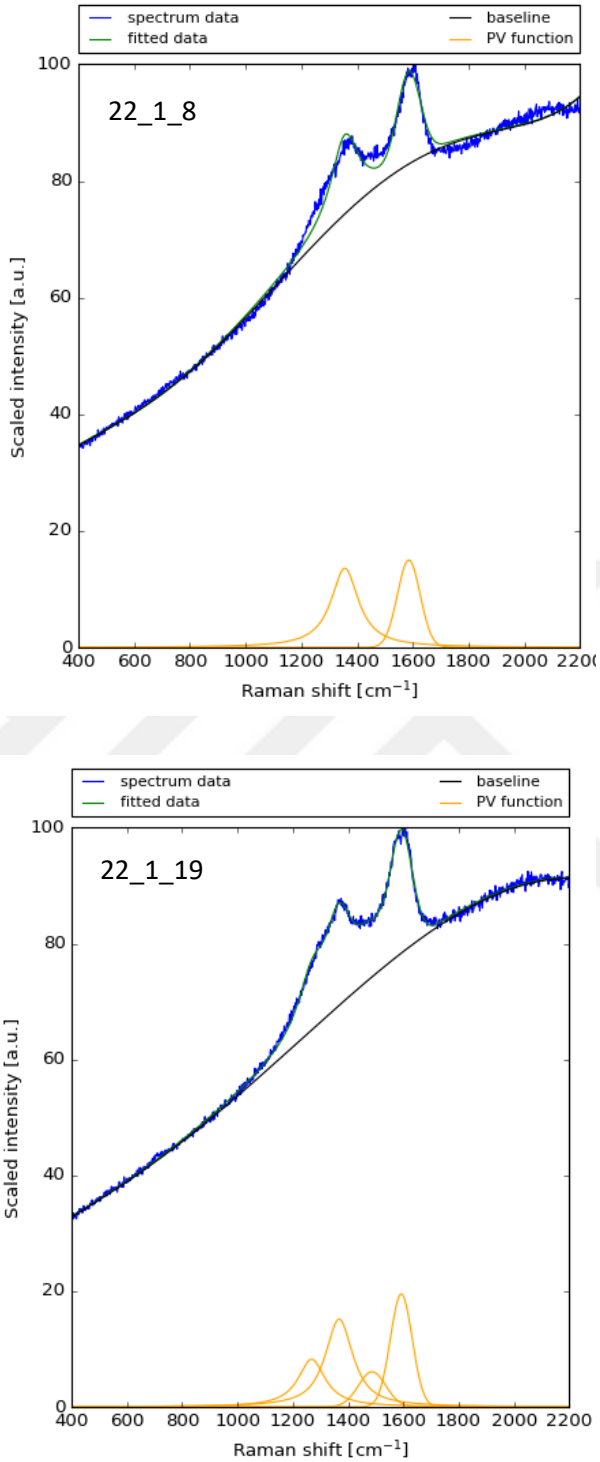

Figure 18. Examples of the D- and G-band curves of 22_1_8 and 22_1_19 fusinite maceral. Deconvolution curves and visuals aregenerated using the Python based IFORS software.

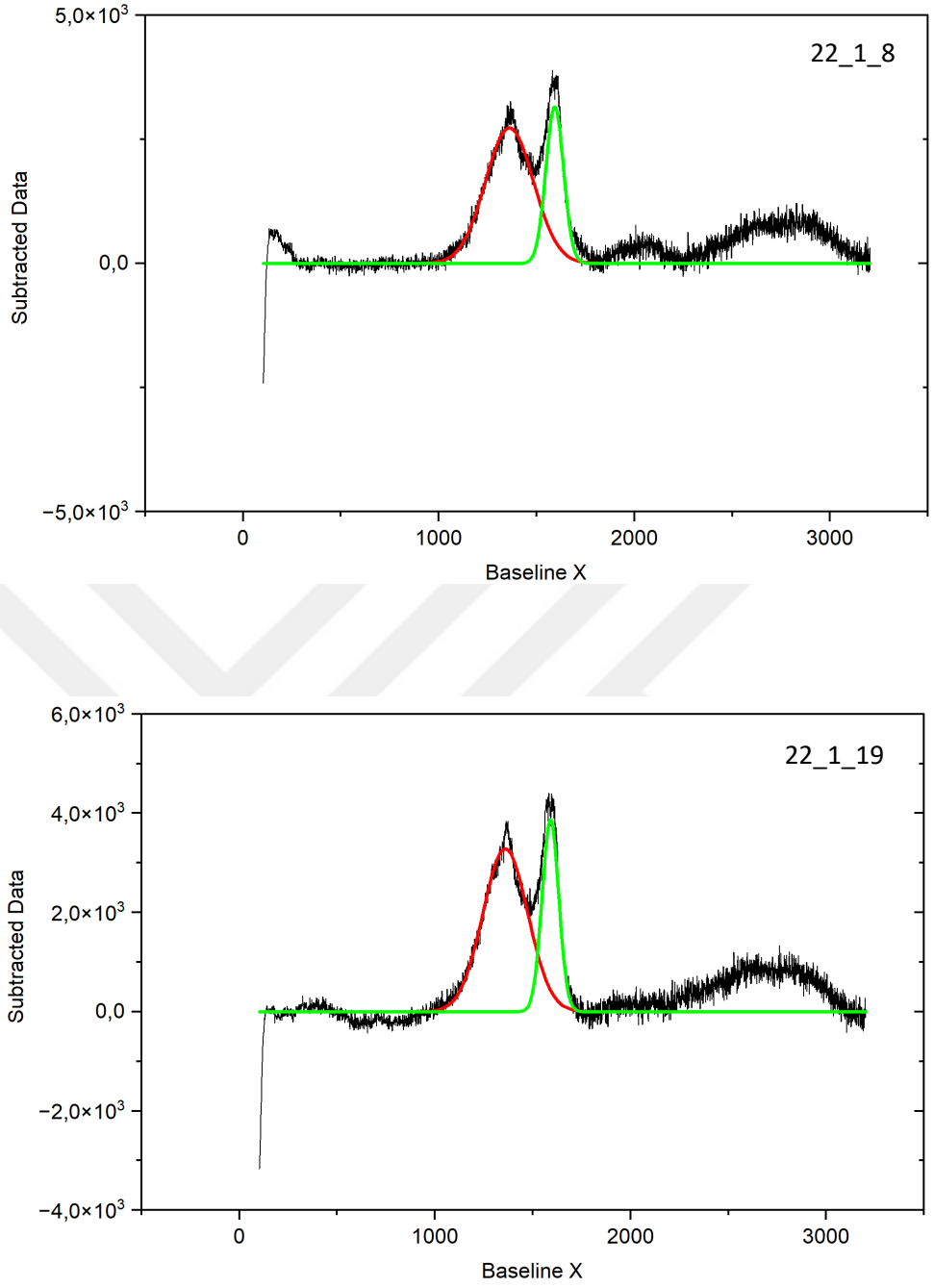

Figure 19. Examples of the D- and G-band curves of 22_1_8 and 22_1_19 fusinite maceral. Deconvolution curves and visuals generated using the OriginPro 2023 software.

Several bi-variate plots are created to evaluate the relations between Raman parameters of fusinite and ulminite (Figs. 21-24) and to analyse the curves obtained from fusinite and ulminite macerals (Appendix-II). R^2 values presented on the figures are based on fusinite macerals since the R^2 values could not be calculated for ulminite due to very low number of data points.

A weak positive correlation is observed in the Area D1 / Area G *versus* Ro graph (R^2 value is 0.41; see Fig. 20). In the Intensity D1/Intensity G *versus* Ro graph (Fig. 21), the values are clustered in the range of 0.80-0.90 and the R^2 value is very low (0.16) indicating no correlation.

The D1 FWHM and G FWHM *versus* Ro graphs (Figs. 22-23) also show no distinctive relations between these parameters.

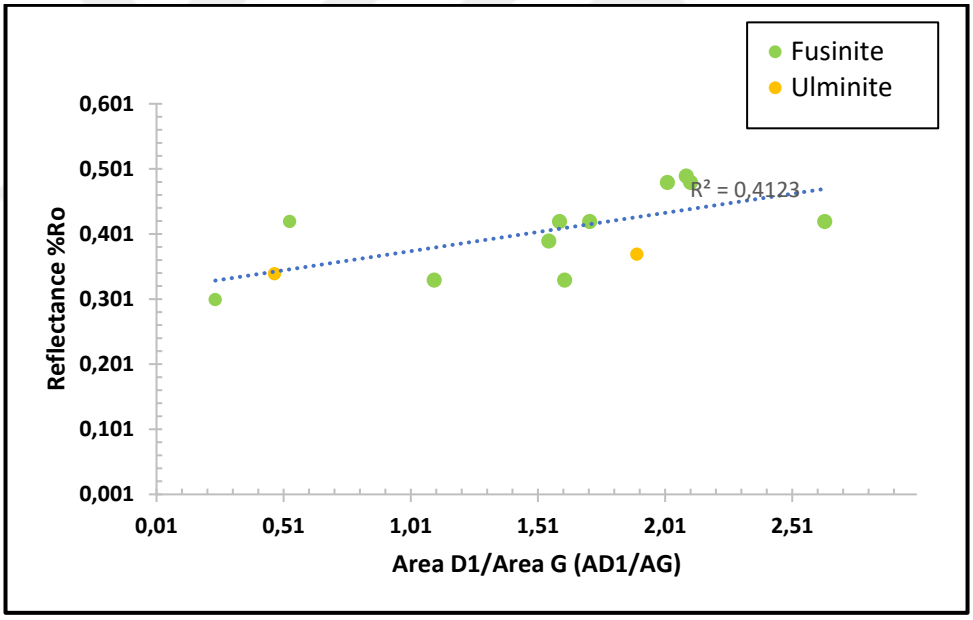

Figure 20. Area D1/Area G versus Reflectance (%Ro) plot.

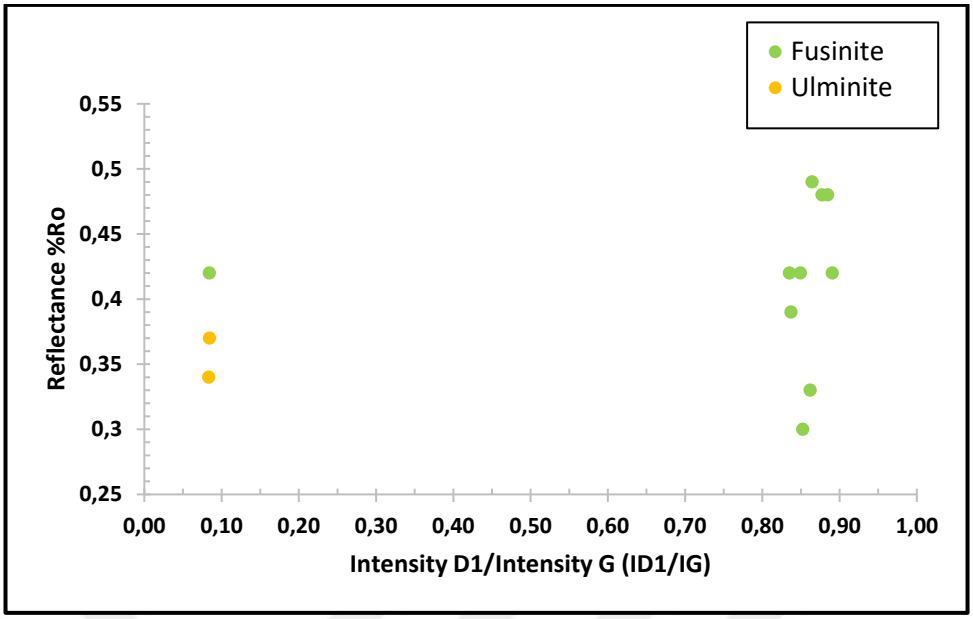

Figure 21. Intensity D1/Intensity G versus Reflectance (%Ro) plot.

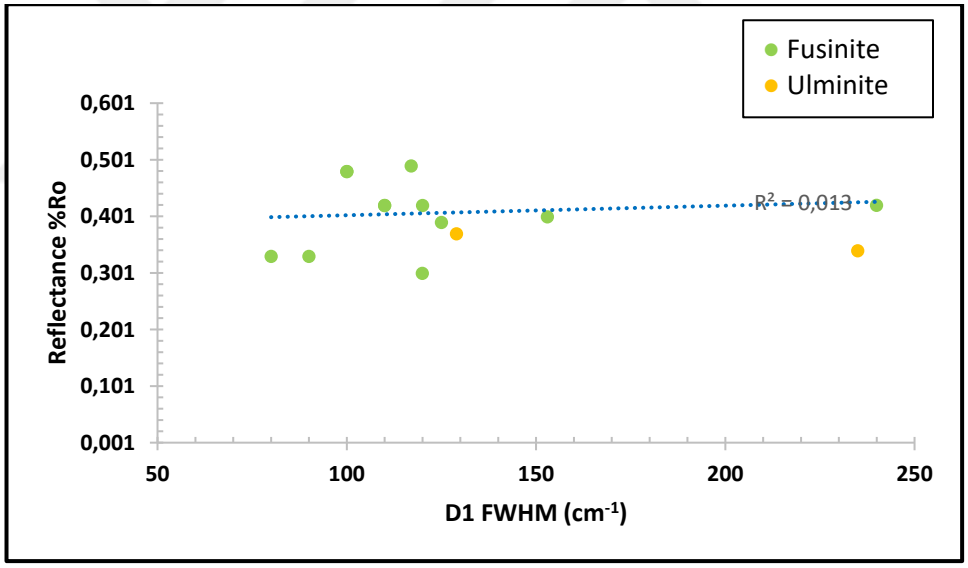

Figure 22. Graph of the Reflectance (%Ro) versus D1 FWHM (FWHM=Width at half height of the peak (cm^{-1})).

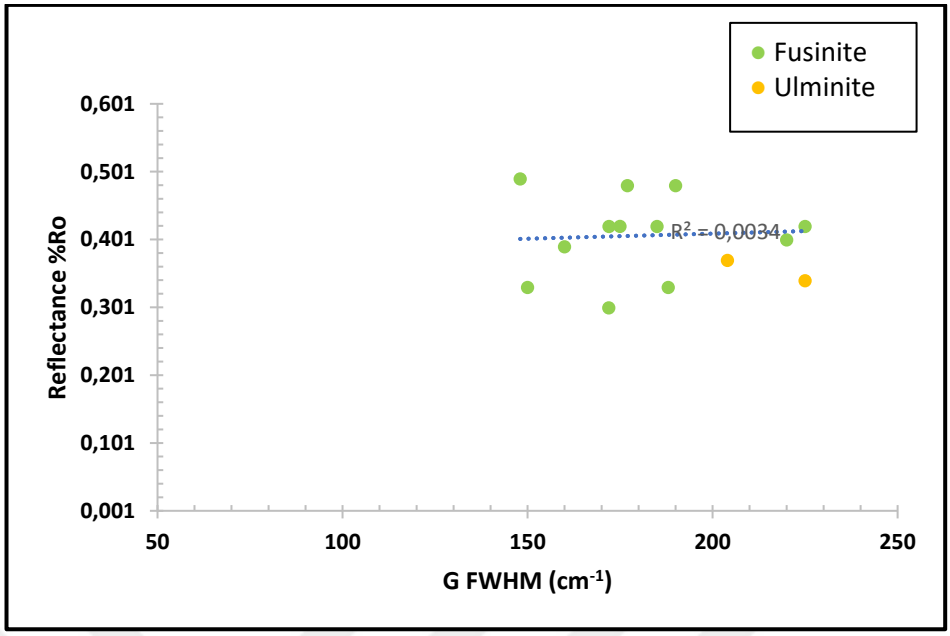

Figure 23. Graph of the Reflectance (%Ro) versus G FWHM (FWHM=Width at half height of the peak (cm^{-1})).

CHAPTER FIVE

DISCUSSIONS AND CONCLUSIONS

The petrographic, mineralogical and geochemical composition of 4 coal samples from a borehole (encoded B-22) in the newly discovered coal field within the Yatağan Thermal Power Plant in Yatağan district of Muğla province are studied and evaluated. Organic petrography, micro-Raman spectroscopy and X-Ray based mineralogical and geochemical approaches are applied. Proximate and calorimetric analyses from earlier work have also been incorporated for complementary evaluation of the gathered data.

The proximate analysis show that, the average total moisture is 5.28%; ash yield 35.38% (dry basis); volatile matter yield 39.23% (dry basis); fixed carbon yield 25.39% (dry basis); total sulfur content 5.47% (dry basis); net calorific value is 16.08 MJ/kg and the gross calorific value is 16.89 MJ/kg. Sample #4 has an ash value of 71.50%; thus, it is not classified as a coal but as carbonaceous rock. Sample #1 has a total sulfur value of 6.68% (dry basis); the reason for the high calorific value of the sample is that sulfur is easily oxidized in the furnace and the oxidation reaction is exothermic, thus adding heat.

Huminite group macerals are common, inertinite and liptinite group macerals are rare and the mineral content varies. It can be interpreted that the coal was formed in an anoxic environment with reed-sedge vegetation and relatively high maceration and bacterial activity.

As indicated earlier, the micro-Raman data evaluated using three different Raman Spectroscopy software present comparable results. The micro-Raman work on the samples was originally planned to be performed on samples #1 and #2, but sample #2 was singed during the analysis process due to high energy, so only one sample was used. A very low number of data points could be obtained from the ulminites due to the hardship of detection under Raman microscope and evaluation of the Raman paremeters could only be completed for a small number of fusinites. The micro-Raman spectroscopy analysis shows that ulminite and fusinite in lignite coal contain a mixture of both disordered (D1 band) and graphitic (G band) carbon structures. Fusinite macerals show steeper peaks (more pronounced hills) than the few ulminites studied. The D1 band shows that ulminites in lignite coal contain significantly irregular carbon structures. Therefore, it may indicate that ulminites are less graphitic and more amorphous

compared to other components. The G band indicates the presence of graphitic carbon structures in the components of lignite coal.

The values of the D1 band of the fusinite macerals vary between 1345 and 1397 cm^{-1} with an average of 1375.17 cm^{-1}. The D1 bands of ulminites range between 1356-1362 cm^{-1} with an average of 1359 cm^{-1}. The peak position averages of the G bands of fusinites and ulminites are determined as 1598.75 cm^{-1} (ranging between 1587-1609 cm^{-1}) and 1593.5 cm^{-1} (ranging between 1593-1594 cm^{-1}), respectively. The D1 and G bands data and characteristics obtained here are within the ranges of values of the coal spectra obtained by Tuinstra and Koenig (1970) and Friedel and Carlson (1971) and is in good agreement with the Raman spectral data of low rank coals elsewhere. Only a weak positive correlation is detected between the fusinite reflectences and the ratios of the areas of the D1 and G Raman bands (AD1/AG) ($r = 0.64$; $R^2 = 0.41$). However, the R^2 value indicates that only 41% of the change in the AD1/AG ratio can elucidate the change in the reflectance values. Still, this result encourages further investigation on larger data sets for elaborating possible relationships between fusinite (and ulminite) reflectance measurements and Raman parameters. The obtained results also contribute to the understanding of the molecular composition and structure of lignite macerals.

XRD analysis of the carbonaceous rock sample shows mainly the presence of mica, quartz, chlorite and calcite and shows that the source of the sedimentary fill in the basin where the lignite deposit is located is the metamorphic series at the basin margin and the basement. Additionally, presence of basaluminite (felsőbányaite) in the XRD spectrum may be considered to be related to weathering of the abundant iron-sulfides (framboidal pyrite) in the studied coal and carbonaceous rock samples. Since high sulfur content can cause slagging, it is important to control this finding by expanding the dataset and take relevant measures.

REFERENCES

Atalay, Z., (1980). Muğla ve Yatağan bölgeleri çevresindeki Neojen yaşlı kıtasal çökellerin stratigrafisi*, Geology Bulletin of Turkey*, 23/1, 93-99.

Azeri, N., (2023). *Triyas-jura yaşlı tabas kömürlerinin kimyasal ve petrografik özellikleri, Orta İran*, [Doctoral dissertation]. Hacettepe University.

Bielowicz, B., & Morga, R. (2021). Micro-raman spectroscopy of selected macerals of the huminite group: An example from the szczerców lignite deposit (central Poland). *Energies*, *14*(2), 281.

Bulut, Y., (2004). *Soma Termik Santralinde Yanan Kömürlerin ve Katı Atıkların Minerolojisi, Petrografisi ve Element İçeriği, Manisa Türkiye*, [Master's thesis] Hacettepe University.

Büçkün, Z., (2013*). Coal Qualıty of the Miocene Muğla-Hüsamlar Lignite*, [Master's thesis], Dokuz Eylül University.

Collins, A. S., & Robertson, A. H. F., (1999). Evolution of the Lycian allochthon, western Turkey, as a northfacing Late Palaeozoic rift and passive continental margin. *Geological Journal,* 34, 107-138.

Çebi, F. H., (2016). Ekizköy (Muğla-Milas) Erken-Orta Miyosen kömürlerinin organik jeokimyası ve paleoiklim şartları. *Journal of Geological Engineering*, 40(2), 209-226.

Erat, S., Telli, A., Ozkendir, O. M., & Demir, B. (2021). Turkey's energy transition from fossil-based to renewable up to 2030: milestones, challenges and opportunities. *Clean Technologies and Environmental Policy*, *23*, 401-412.

Erecek, B. (2020). *Muğla-Yatağan Güneybatısında Yer Alan (Şahinler-Bozüyük Arası) Linyit Sahasının Kömür Petrografisinin İncelenmesi,* [Unpublished thesis], Dokuz Eylül University.

Erecek, B., Akbulut, M., Christanis, K., & İnaner, H. (2023, April 10-14). *Muğla-Yatağan Şahinler-Bozüyük Kömür Sahası (GB Türkiye) B-22 Sondajı Örneklerinin Petrografik, Mineralojik ve Jeokimyasal Bileşimi* [Conference presentation abstract]. Seventy-fifth Geological Congress of Türkiye with International Participation, Ankara, Türkiye. https://www.jmo.org.tr/resimler/ekler/24f25904af8a59f_ek.pdf

Friedel, R. A., & Carlson, G. L. (1972). Difficult carbonaceous materials and their infra-red and Raman spectra Reassignments for coal spectra. *Fuel*, *51*(3), 194-198.

General Directorate of Mineral Research and Exploration (MTA). (2010). Inventory of Turkish lignites: MTA Publication, (in Turkish).

Graciansky, P. C., (1972). Reserches geologiques dans le Taurus Lycien occidental. [Master's thesis]. University de Paris-Sud.

Green, P. D., Johnson, C. A., & Thomas, K.M. (1983). Applications of laser Raman microprobe spectroscopy to the characterization of coal and cokes. *Fuel, 62,* 1013-1023.

Gürsoy, E.M., Ünal, D., Tan, T., Sun, S., Karahan, Ç., Aydın, H., et.al. (1993). Inventory of Coal. İzmir: MTA Aegean Regional Directorate, (in Turkish).

Guedes, A., Valentim, B., Prieto, A. C., Rodrigues, S., & Noronha, F. (2010). Micro-Raman spectroscopy of collotelinite, fusinite and macrinite. *International Journal of Coal Geology*, *83*(4), 415-422.

Gomez, A. B., Kataitzidis, S., & Wagner, N., (2022), Course organic petrology.

ICCP Course Book.

Hacımustafaoğlu, I., Akbulut, M., İnaner, H., Chrisranis, K. (2023, April 10-14). *Şahinler–Bozüyük Linyit Yatağının (Muğla-Yatağan, GB Türkiye) Jeolojik Konumu ve Hüminit Yansıtmalarının Ölçümü* [Conference presentation abstract]. Seventy-fifth Geological Congress of Türkiye with International Participation, Ankara, Türkiye. https://www.jmo.org.tr/resimler/ekler/24f25904af8a59f_ek.pdf

Henry, D.G., Jarvis, I., Gillmore, G., Stephenson, M., & Emmings, J., (2018). Assessing lowmaturity organic matter in shales using Raman spectroscopy: Effects of sample preparation and operating procedure. Int. J. Coal Geol. 191, 135–151.

Henry, D. G., Jarvis, I., Gillmore, G., & Stephenson, M. (2019a). Raman spectroscopy as a tool to determine the thermal maturity of organic matter: Application to sedimentary, metamorphic and structural geology. *Earth-Science Reviews*, *198*, 102936.

Henry, D.G., Jarvis, I., Gillmore, G., & Stephenson, M., (2019b). A rapid method for determining organic matter maturity using Raman spectroscopy: Application to Carboniferous organic-rich mudstones and coals. Int. J. Coal Geol. 203, 87–98.

İnaner, H., (1994). *Güneybatı Anadolu Linyit Havzalarının Değerlendirilmesi* [Unpublished doctoral dissertation]. Dokuz Eylül University.

Khatibi, S., Ostadhassan, M., Tuschel, D., Gentzis, T., & Carvajal-Ortiz, H., (2018). Evaluating molecular evolution of kerogen by Raman spectroscopy: Correlation with optical microscopy and Rock-Eval pyrolysis. Energies 11, 1406.

Koçyiğit, A., Yusufoğlu, H., & Bozkurt, E. (1999). Evidence from the Gediz graben for episodic two-stage extension in western Turkey. *Journal of the Geological Society,* 156 (3), 605-616.

Koç, Ç. S. (2017). *Tınaz (Muğla-Yatağan) ve çevresindeki kömür içerikli tortulların paleoflorası ve paleoiklimi* [Master's thesis]. Ege University.

Kürçer, A., & Gürsoy, H. (2023). Yatağan fayının aktif tektonik özellikleri ve Holosen paleosismolojik tarihçesi, Güneybatı Anadolu, Türkiye. *MTA Journal of Geosciences and Mining*, 2(2), 87-112.

Li, X., Hayashi, J. I., & Li, C. Z. (2006). Volatilisation and catalytic effects of alkali and alkaline earth metallic species during the pyrolysis and gasification of Victorian brown coal. Part VII. Raman spectroscopic study on the changes in char structure during the catalytic gasification in air. *Fuel*, *85*(10-11), 1509-1517.

Lünsdorf, N. K., Dunkl, I., Schmidt, B. C., Rantitsch, G., & von Eynatten, H. (2017). Towards a higher comparability of geothermometric data obtained by Raman spectroscopy of carbonaceous material. Part 2: A revised geothermometer. *Geostandards and Geoanalytical Research*, *41*(4), 593-612.

Nakoman, E., (1978). Paleocoğrafik Verilerin Kömür Aramalarındaki Önemi Üzerine Bir Araştırma. *Türkiye I. Coal Congress*, Zonguldak-Türkiye.

Nakoman, E., (1982), *Coal Deposits of Turkey* [Unpublished doctoral dissertation]. Dokuz Eylül University.

Nakoman, E., & İnaner, H., (1990), Lignite Deposits of Southwestern Türkiye. *International Earth Sciences Congress on Aegean Regions*, İzmir-Türkiye.

Mukhopadhyay, P. (1989). Organic petrography and organic geochemistry of Tertiary coals from Texas in relation to depositional environment and hydrocarbon generation. Report of Investigations. Bureau of Economic Geol., Texas. 118 pp.

Oberhänsli, R., Partzsch, J., Candan, O., & Etünkaplan, M., (2001). First occurrence of Fe-Mg-caroholite documenting high-pressure metamorphism in metasediments of the Lycian Nappes, SW Turkey. *International Journal of Earth Sciences*, 89, 867- 873.

OTTO-GOLD, (1965), *Linyit Etüdü (Jeoloji)*, Cilt II, MTA Publish, Ankara.

Palache, C., Berman, H., & Frondel, C. (1951). The System of Mineralogy of JD Dana and ES Dana, 7th Edit. https://handbookofmineralogy.org/pdfs/basaluminite.pdf

Potgieter-Vermaak, S., Maledi, N., Wagner, N., Van Heerden, J. H. P., Van Grieken, R., & Potgieter, J. H. (2011). Raman spectroscopy for the analysis of coal: a review. *Journal of Raman Spectroscopy*, 42(2), 123-129.

Querol, X., Alastuey, A., Plana, F., Lopez-Soler, A., Tuncali, E., Toprak, S., et.al. (1999). Coal geology and coal quality of the Miocene Mugla basin, southwestern Anatolia, Turkey. *International Journal of Coal Geology*, *41*(4), 311-332.

Schito, A., & Corrado, S. (2020). An automatic approach for characterization of the thermal maturity of dispersed organic matter Raman spectra at low diagenetic stages. Geological Society, London, Special Publications, 484(1), 107-119.

Schito, A., & Corrado, S. (2020). An automatic approach for characterization of the thermal maturity of dispersed organic matter Raman spectra at low diagenetic stages. *Geological Society, London, Special Publications*, *484*(1), 107-119.

Schmidt, J.L., Hinrichs, R., Araujo, C.V., (2017). Maturity estimation of phytoclasts in strew mounts by micro-Raman spectroscopy. Int. J. Coal Geol. 173, 1–8.

Scott, A. C. (2002). Coal petrology and the origin of coal macerals: a way ahead? *International Journal of Coal Geology, 50*, 119-134.

Sözbilir, H., (2002). Geometry and origin of folding in the Neogene sediments of the Gediz Graben, western Anatolia, Turkey. *Geodinamica Acta* 15 (5–6), 277–288.

Sýkorová, I., Pickel, W., Christanis, K., Wolf, M., Taylor, G.H. & Flores, D. (2005). Classification of Huminite – ICCP System 1994. *International Journal of Coal Geology*, 62, 85-106.

Taylor, G.H., Teichmüller, M., Davis, A., Diessel, C.F.K., Littke, R. & Robert, P. (1998). Organic Petrology. A New Handbook incorporating some revised parts of Stach's Textbook of Coal Petrology. *Geological Magazine*, 136(6), 697-711.

Toprak, S., (1996), Alpagut-Dodurga (Osmancık-Çorum) Bölgesi Çevresindeki Kömürlerin Oluşum Ortamları ve Özelliklerinin Belirlenmesi [Doctoral dissertation]. Hacettepe University.

Tuinstra, F., & Koenig, J. L. (1970). Raman spectrum of graphite. *The Journal of chemical physics*, *53*(3), 1126-1130.

Ünal, D., (1987), Muğla-Milas Sekköy-Ekizköy (Karacaağaç Bölümü) Linyit Sektörü 1987 Yılı Çalışma Raporu. *Mineral Research and Exploration Institute of Turkey (MTA) report.*

Ünal, D., (1989), Muğla-Tınaz-Bağyaka Linyit Sektörü 1988 Yılı Çalışmaları Jeoloji Raporu. *Mineral Research and Exploration Institute of Turkey (MTA) report.*

Ünalan, G., (2010), Kömür Jeolojisi. *Maden Tetkik ve Arama Genel Müdürlüğü, Education Series-41*,

Ward, C.R., (1984), Coal Geology and Coal Technology, Blackwell Sci. Publ., London.

Yakupoğlu, T., & Bayhan, E. (2017). Yatağan (Muğla/GB Türkiye) Civarındaki Neojen Yaşlı Sedimanter Kayaçların Sedimantolojik ve Sedimanter Petrografik Özellikleri. *Yüzüncü Yıl Üniversitesi Journal of the Institute of Science and Technology*, 22(2), 120-131.

Wilkins, R.W.T., & Sherwood, N., Li, Z., (2018). RaMM (Raman maturity method) study of samples used in an interlaboratory exercise on a standard test method for determination of vitrinite reflectance on dispersed organic matter in rocks. Mar. Pet. Geol. 91, 236–250.

Yiğitel, I., (1979), Güneybatı Anadolu'da yer alan sahaların genel görünümü, *Mineral Research and Exploration Institute of Turkey (MTA) report.*

Zerda, T. W., John, A., & Chmura, K. (1981). Raman Studies of Coals. *Fuel*, *60*(5), 375-378.

APPENDIX I

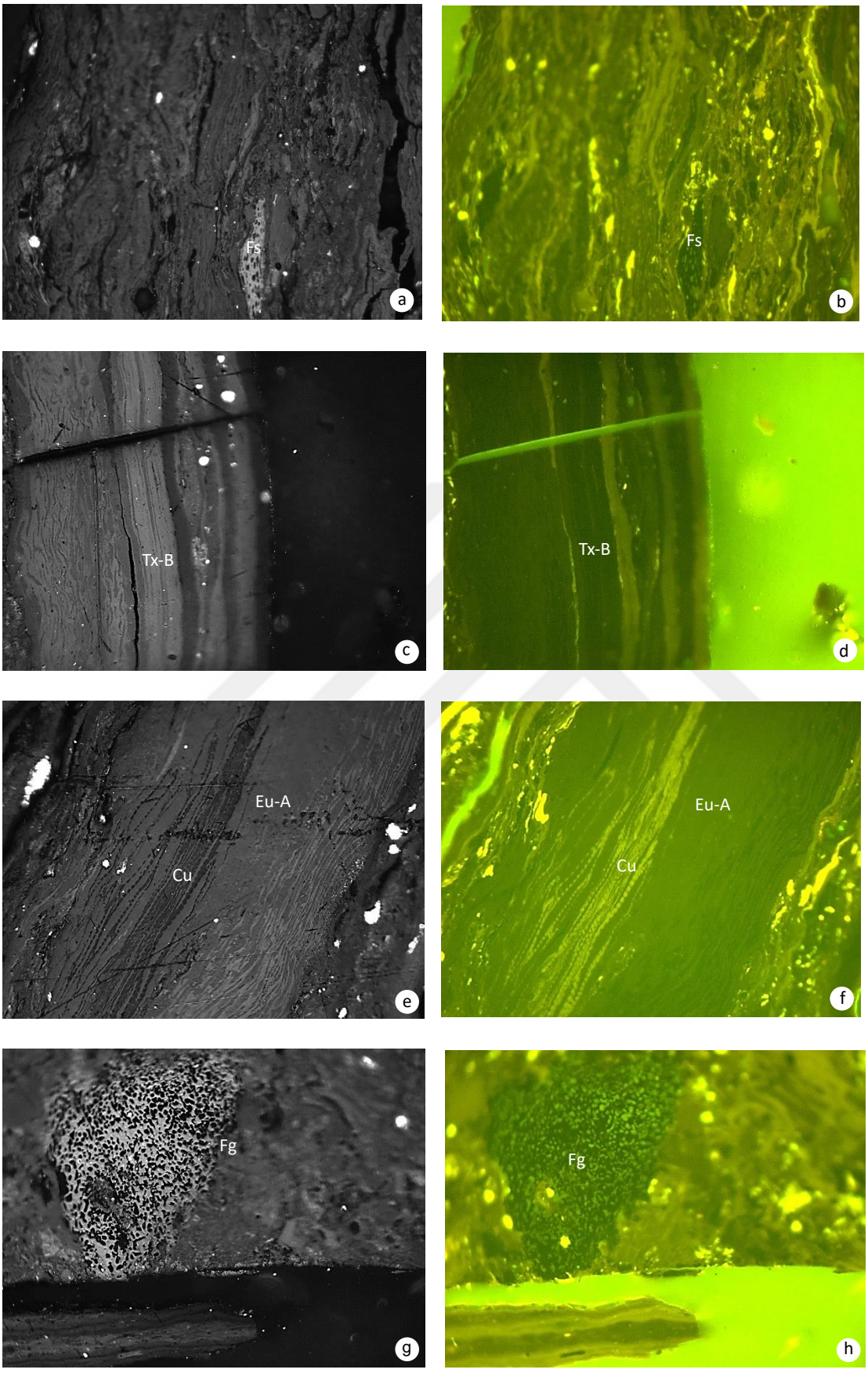

Plate 1. Photomicrographs of sample #1 under incident white light and blue-light excitation, oil immersion, 500X total magnification.

Plate 1. Sample number 1's macerals under white (a, c, e, g) and ultraviolet light (b, d, f, h) at 500x magnification. Each photograph has a long side of 230 μm and a short side of 173 μm.

a. and b. Fusinite (Fs).

c. and d. Textinite B (Tx-B).

e. and f. Eu-Ulminite A (Eu-A), Cutinite (Cu).

g. and h. Funginite (Fg).

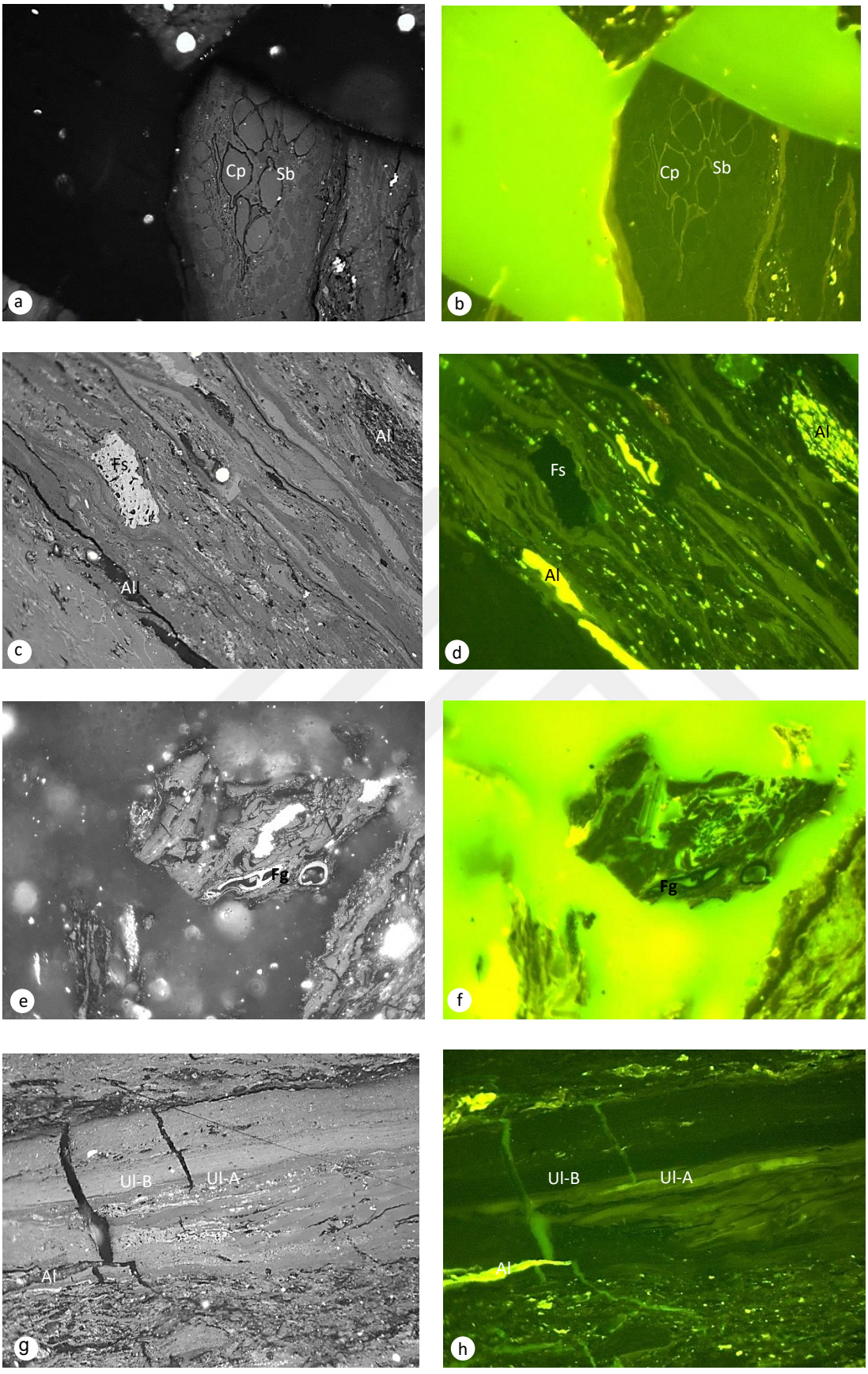

Plate 2. Photomicrographs of sample #1 and #2 under incident white light and blue-light excitation, oil immersion, 500X total magnification.

Plate 2. Sample number 1 and 2 macerals under white (a, c, e, g) and ultraviolet light (b, d, f, h) at 500x magnification. Each photograph has a long side of 230 μm and a short side of 173 μm.

a. and b. Corpohuminite (Cp), Suberinite (Sb) (Sample 1).

c. and d. Alginite (Al) (Sample 1).

e. and f. Funginite (Fg) (Sample 2).

g. and h. Ulminite-A (Ul-A), Ulminite-B (Ul-B) (Sample 2).

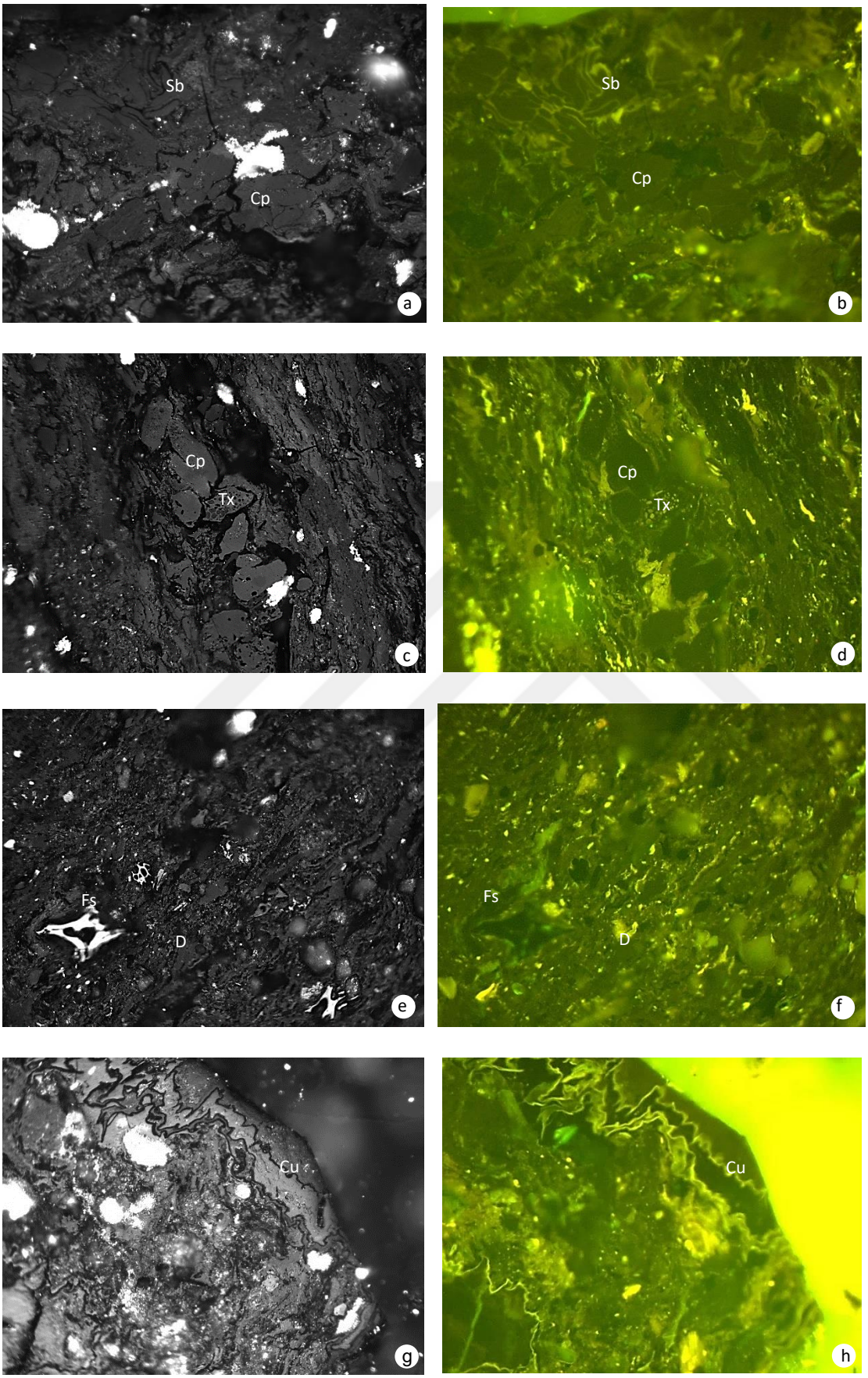

Plate 3. Photomicrographs of sample #3 and #4 under incident white light and blue-light excitation, oil immersion, 500X total magnification.

Plate 3. Sample number 3 and 4 macerals under white (a, c, e, g) and ultraviolet light (b, d, f, h) at 500x magnification. Each photograph has a long side of 230 μm and a short side of 173 μm.

a. and b. Corpohuminite (Cp), Suberinite (Sb) (Sample 3).

c. and d. Corpohuminite (Cp), Textinite (Tx) (Sample 3).

e. and f. Fusinite (Fs), Densinite (D) (Sample 3).

g. and h. Cutinite (Cu) (Sample 4).

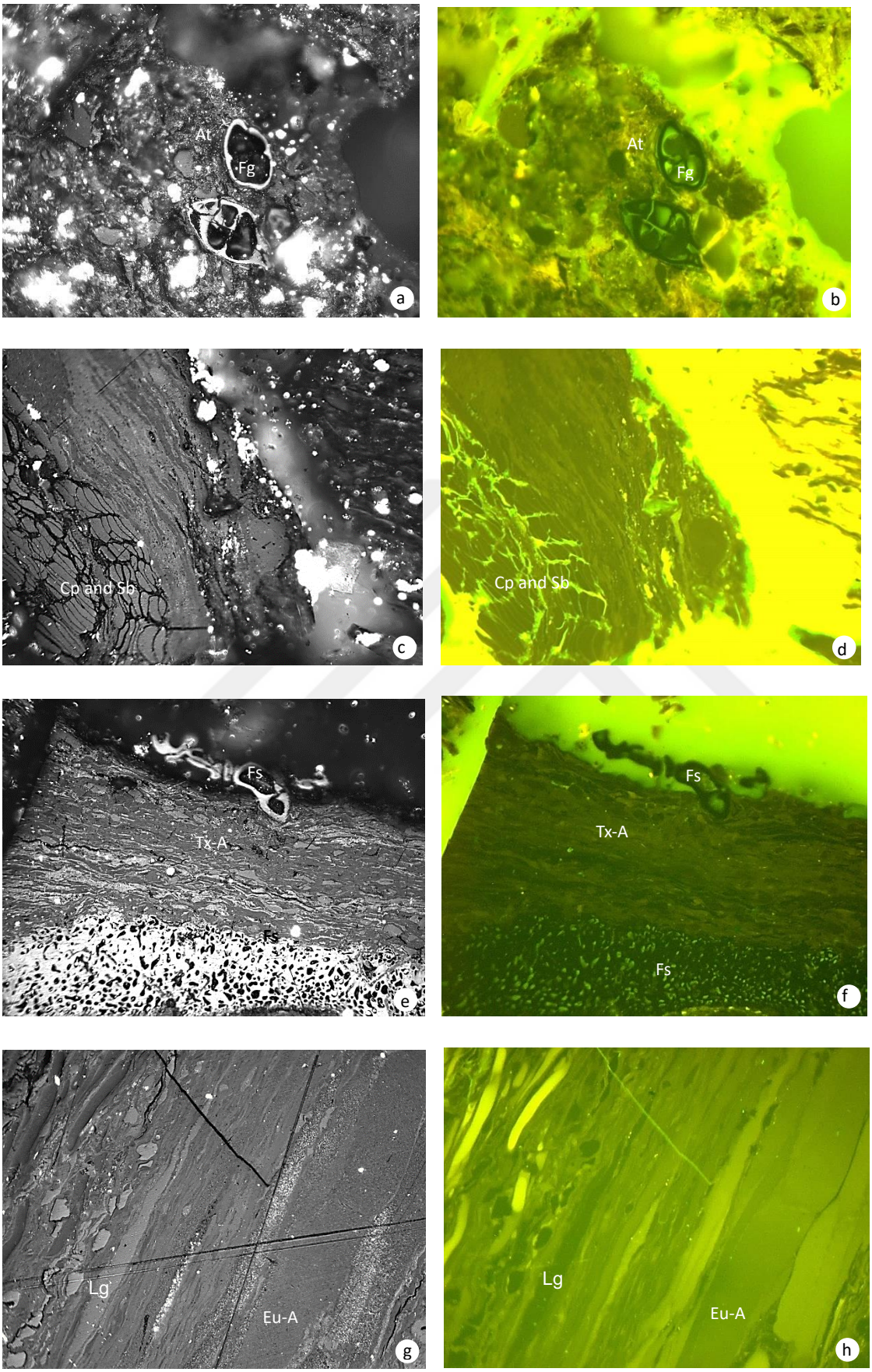

Plate 4. Photomicrographs of sample #4 under incident white light and blue-light excitation, oil immersion, 500X total magnification.

Plate 4. Sample number 4 macerals under white (a, c, e, g) and ultraviolet light (b, d, f, h) at 500x magnification. Each photograph has a long side of 230 μm and a short side of 173 μm.

a. and b. Funginite (Fg), Atrinite (At).

c. and d. Corpohuminite (Cp), Suberinite (Sb).

e. and f. Textinite-A (Tx-A).

g. and h. Levigelite (Lg), Eu-Ulminite (Eu-A)

APPENDIX II

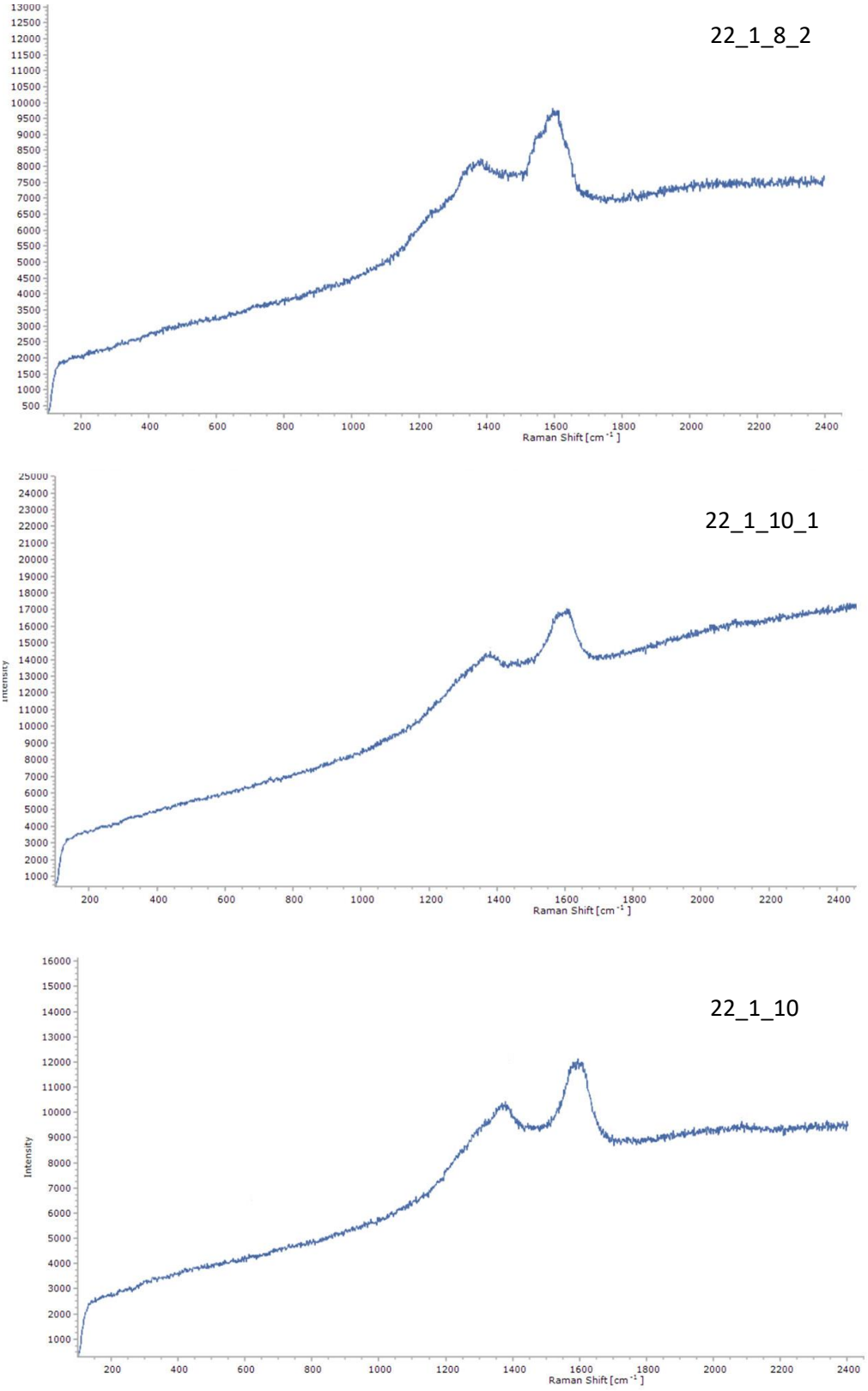

Plate 5. D1 and G peak parameters of samples from SpectraGryph.

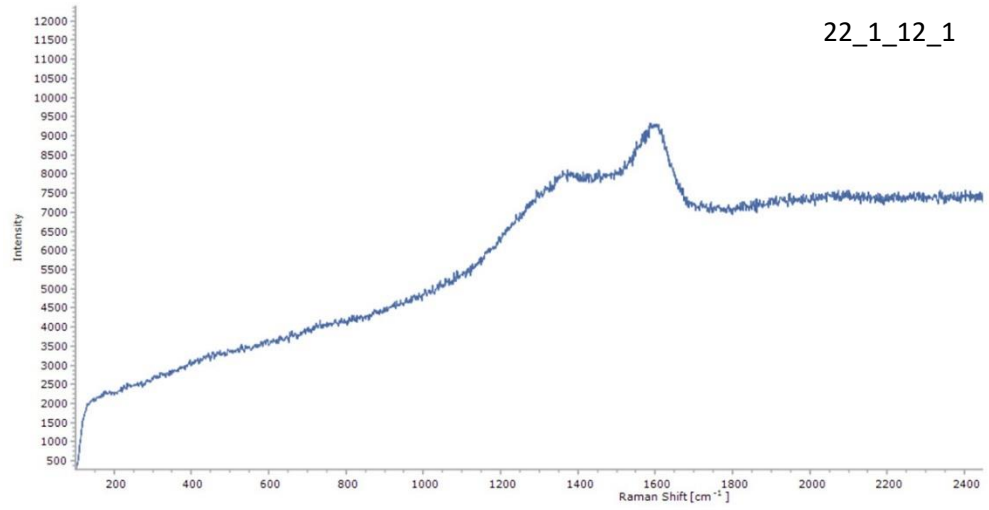

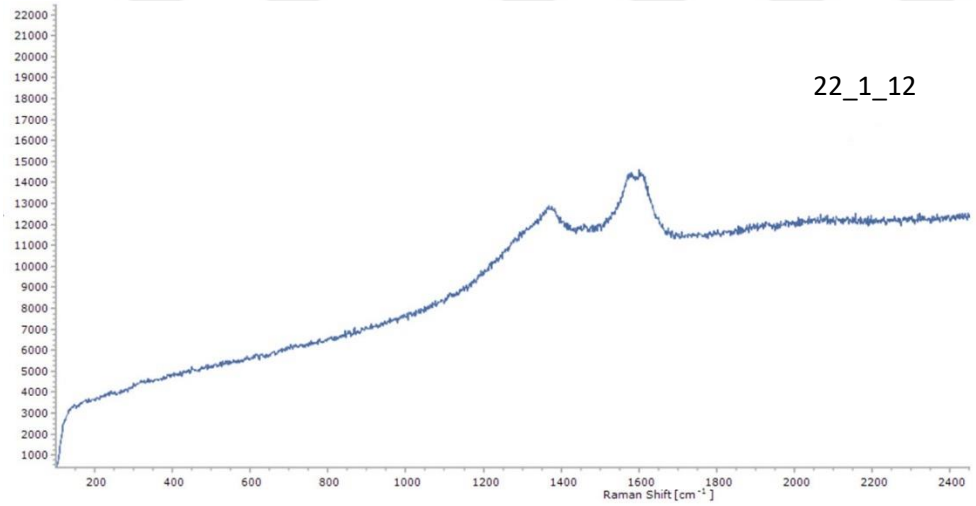

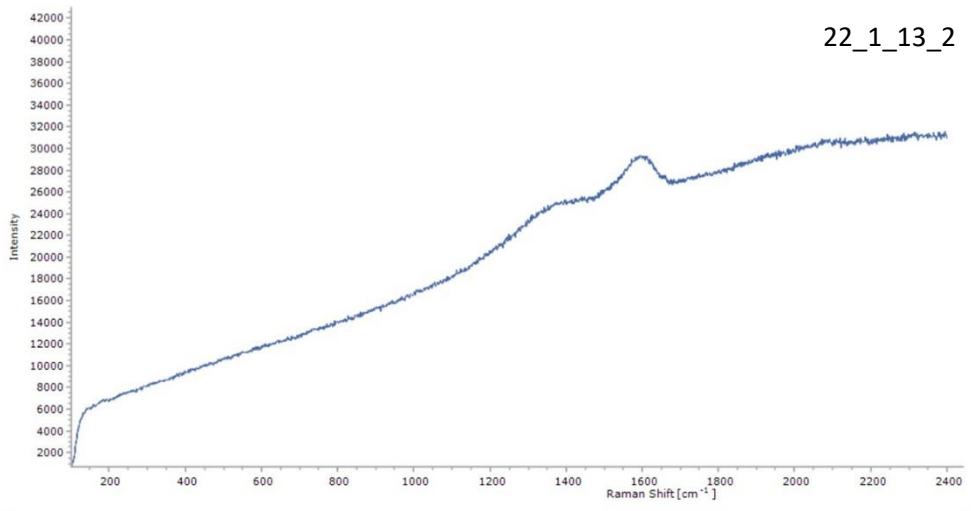

Plate 6. D1 and G peak parameters of samples from SpectraGryph.

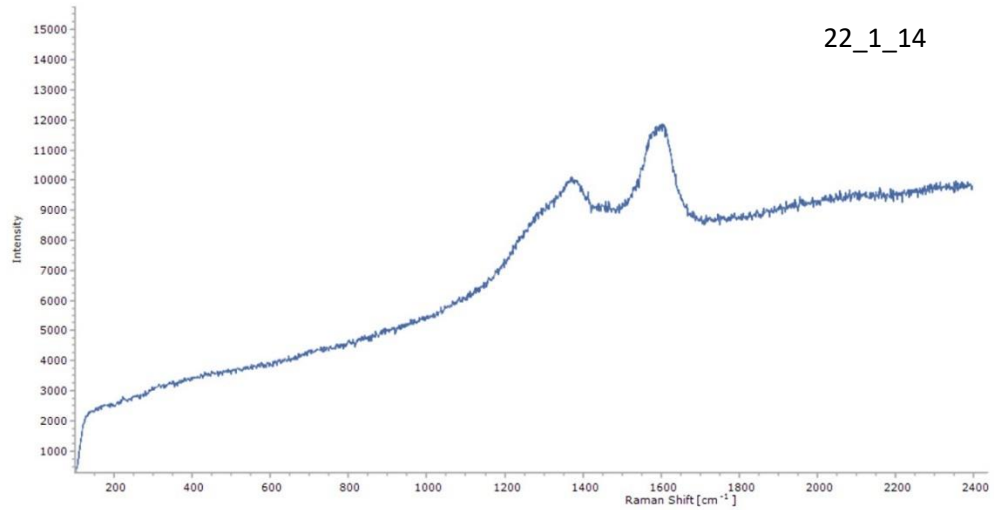

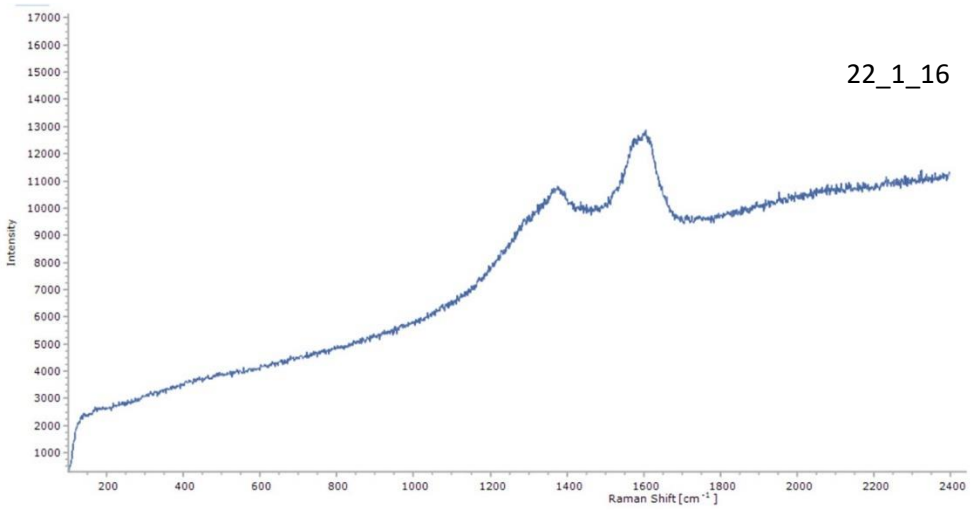

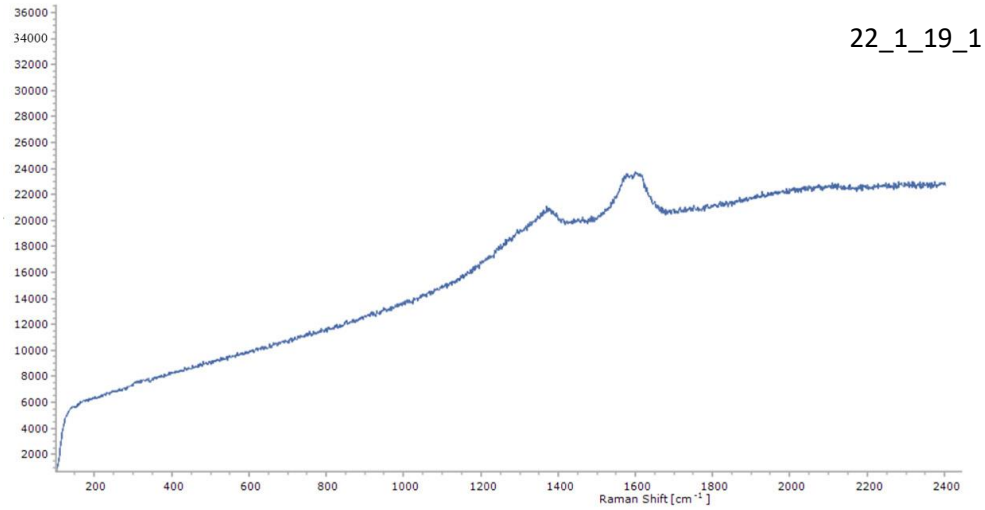

Plate 7. D1 and G peak parameters of samples from SpectraGryph.

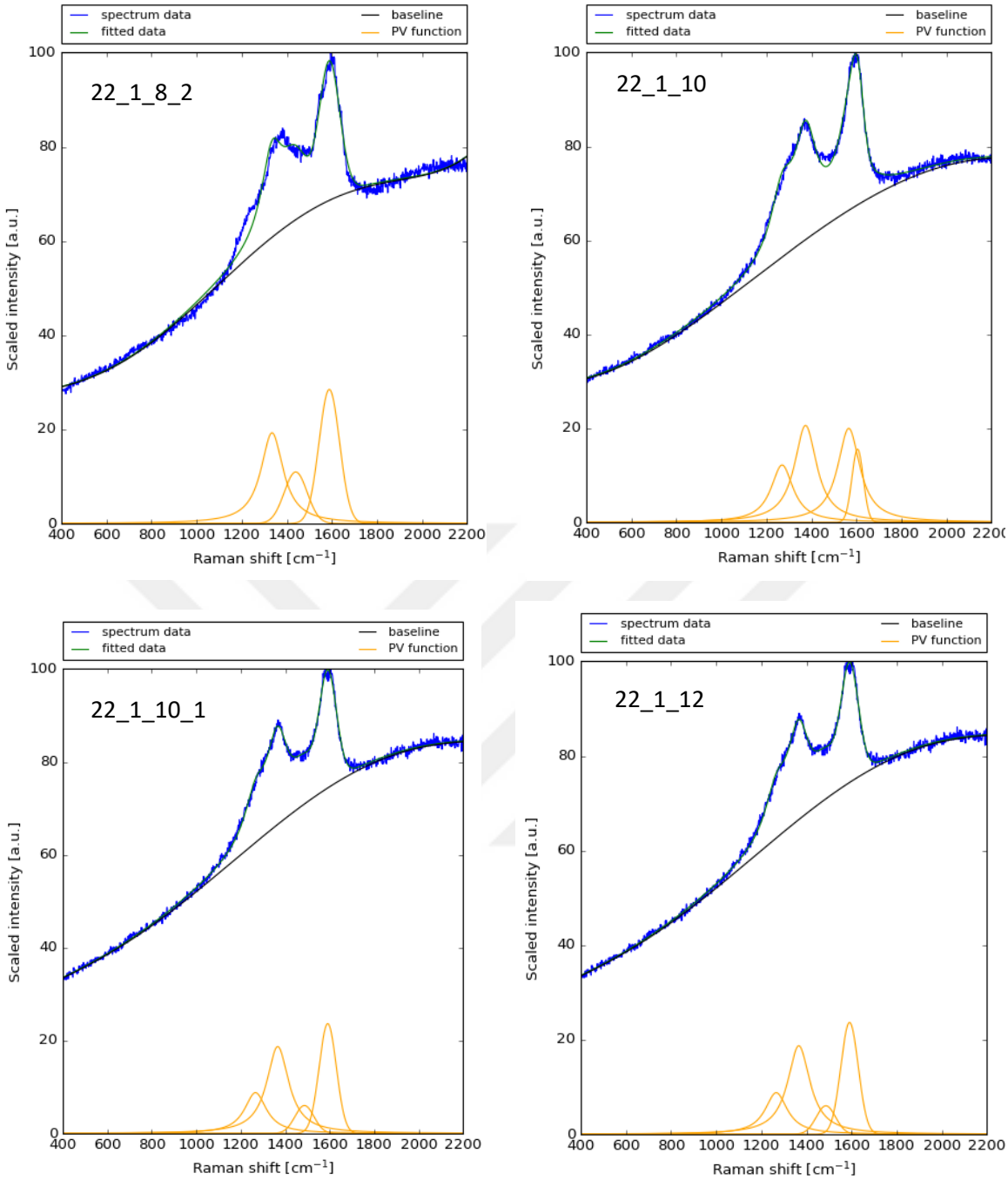

Plate 8. D1 and G peak parameters of samples from IFORS.

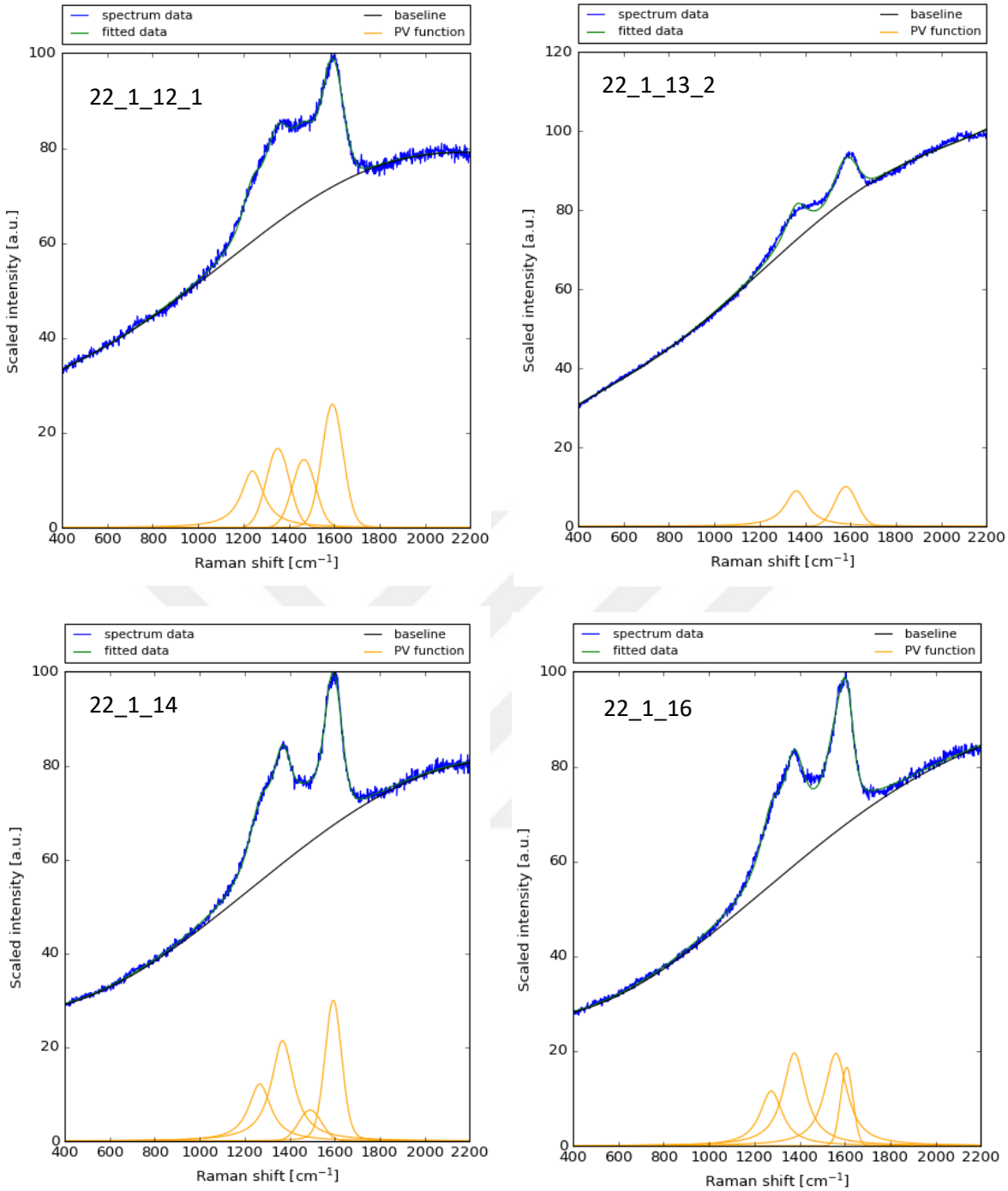

Plate 9. D1 and G peak parameters of samples from IFORS.

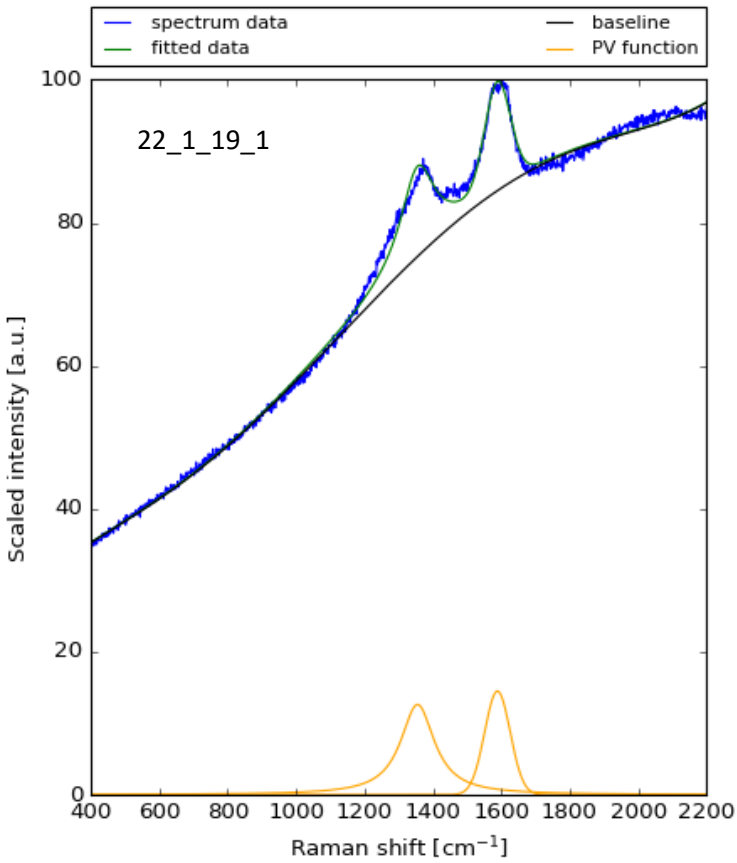

Plate 10. D1 and G peak parameters of sample from IFORS.

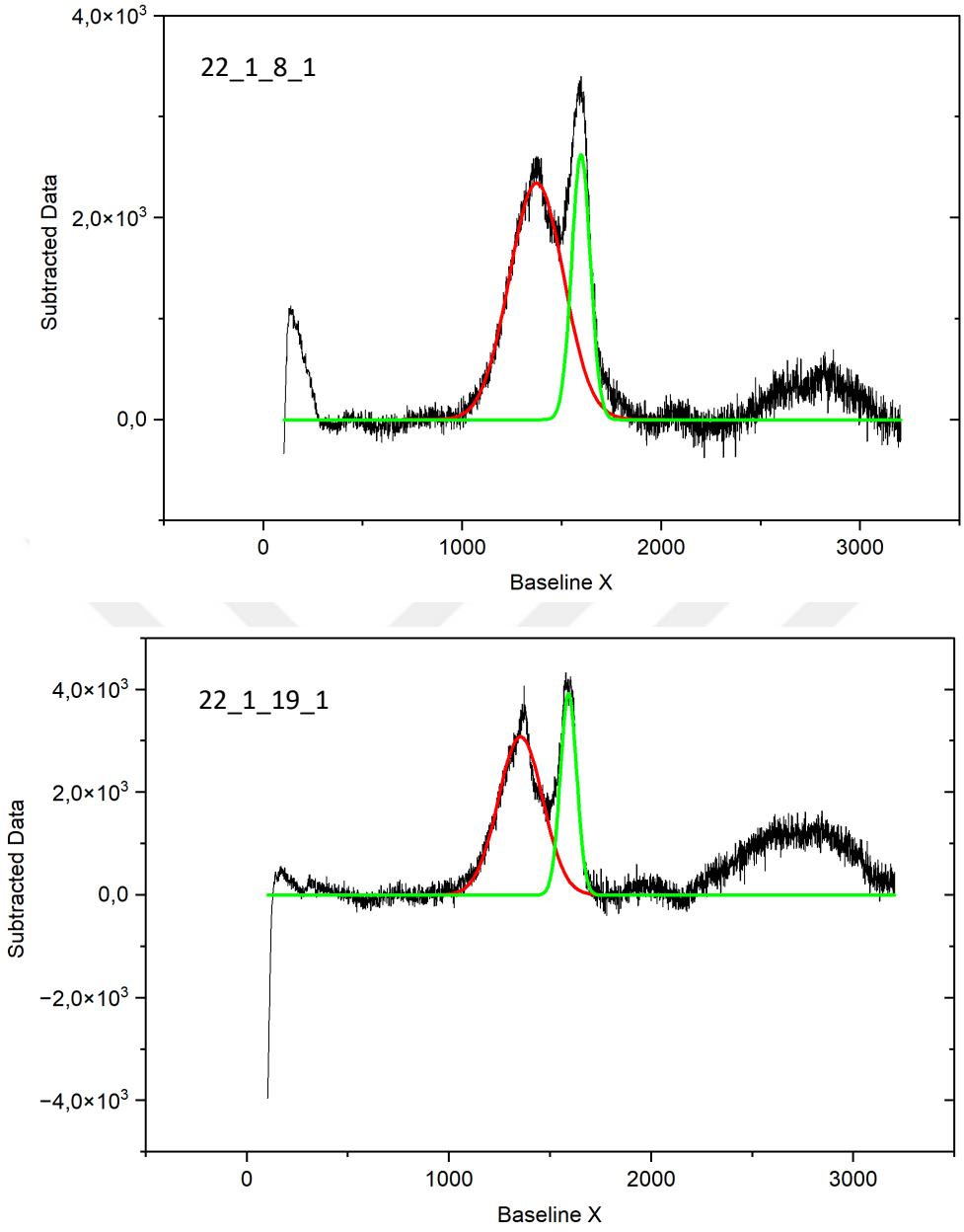

Plate 11. D1 and G peak parameters of samples from OriginPro.

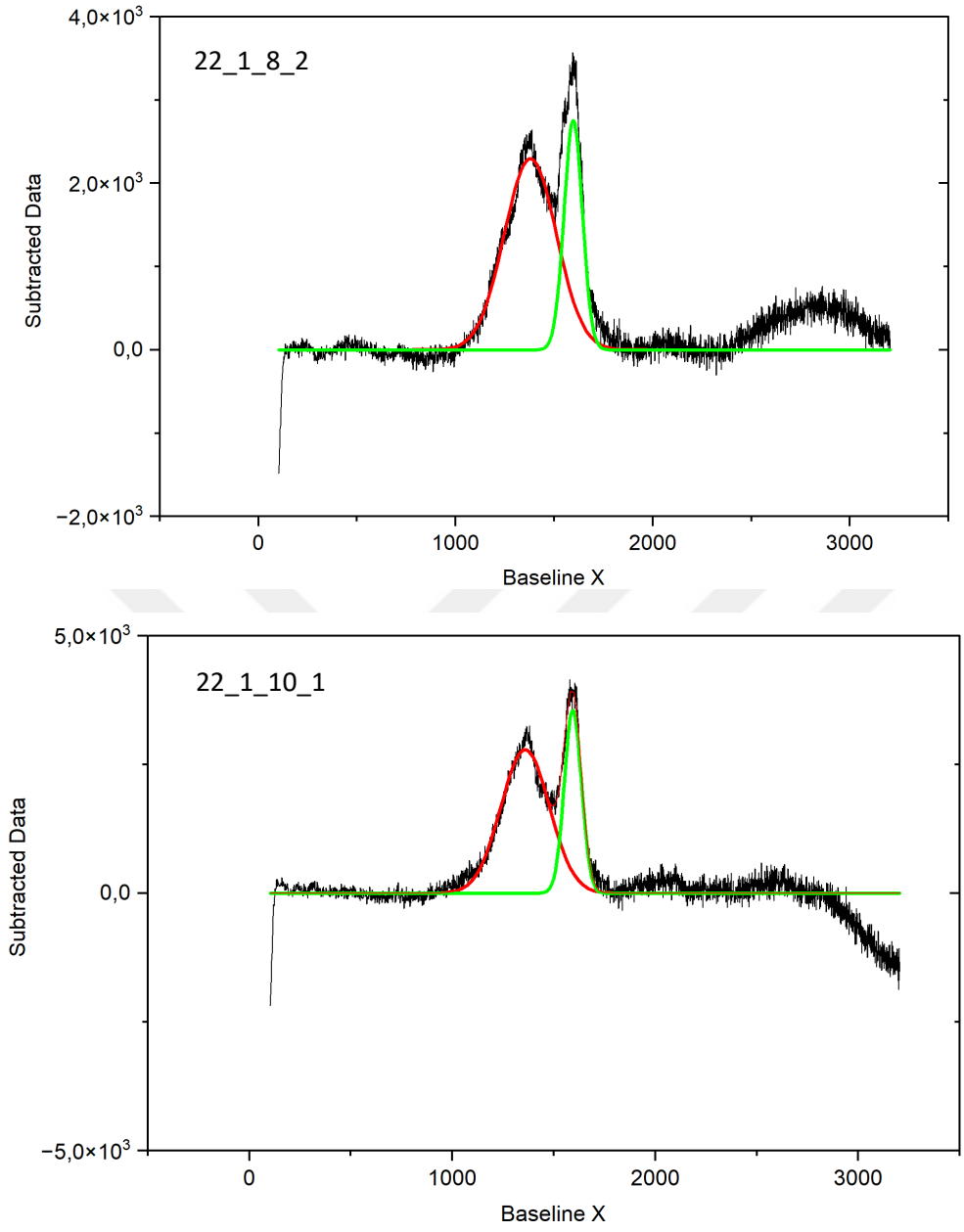

Plate 12. D1 and G peak parameters of samples from OriginPro.

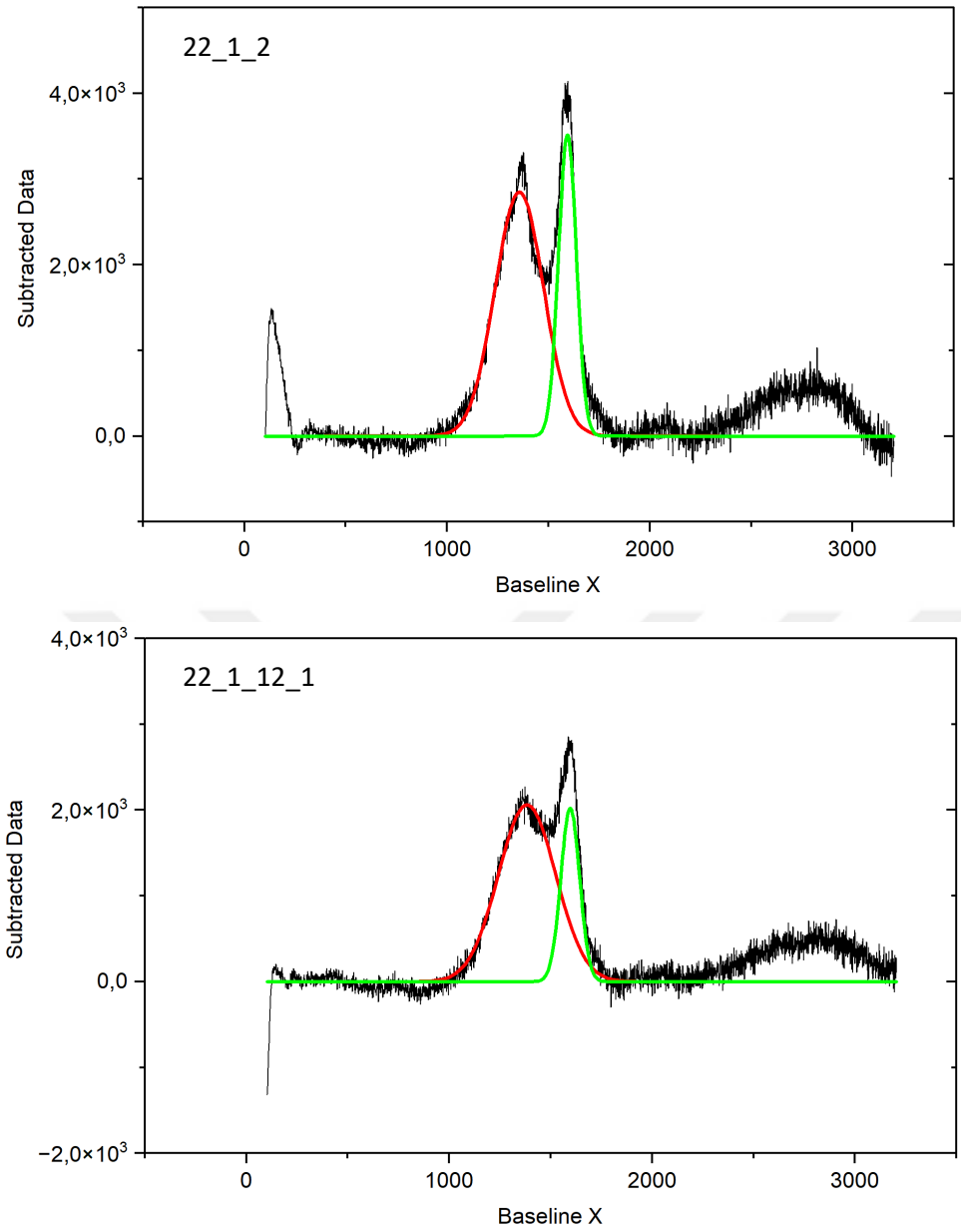

Plate 13. D1 and G peak parameters of samples from OriginPro.

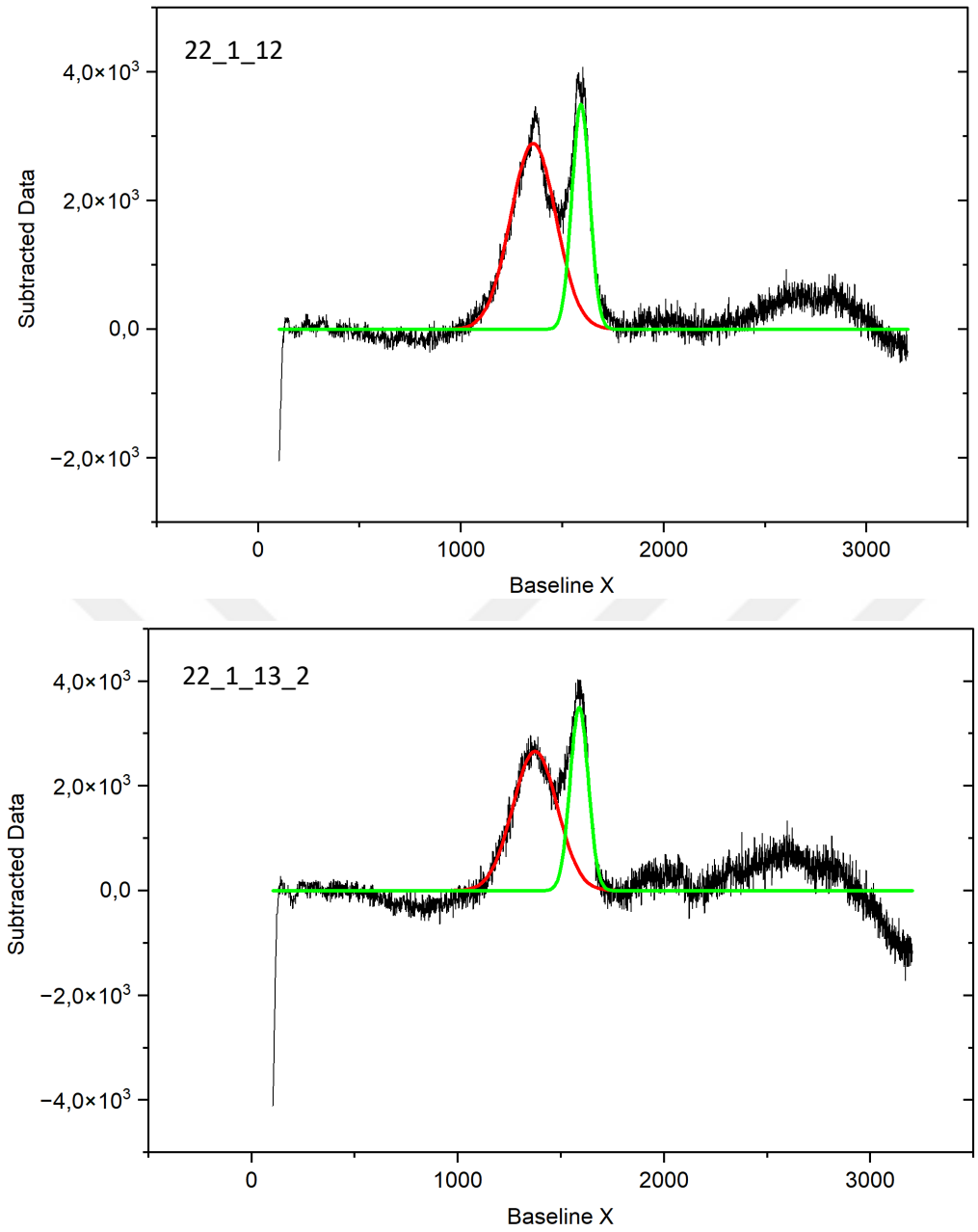

Plate 14. D1 and G peak parameters of samples from OriginPro.

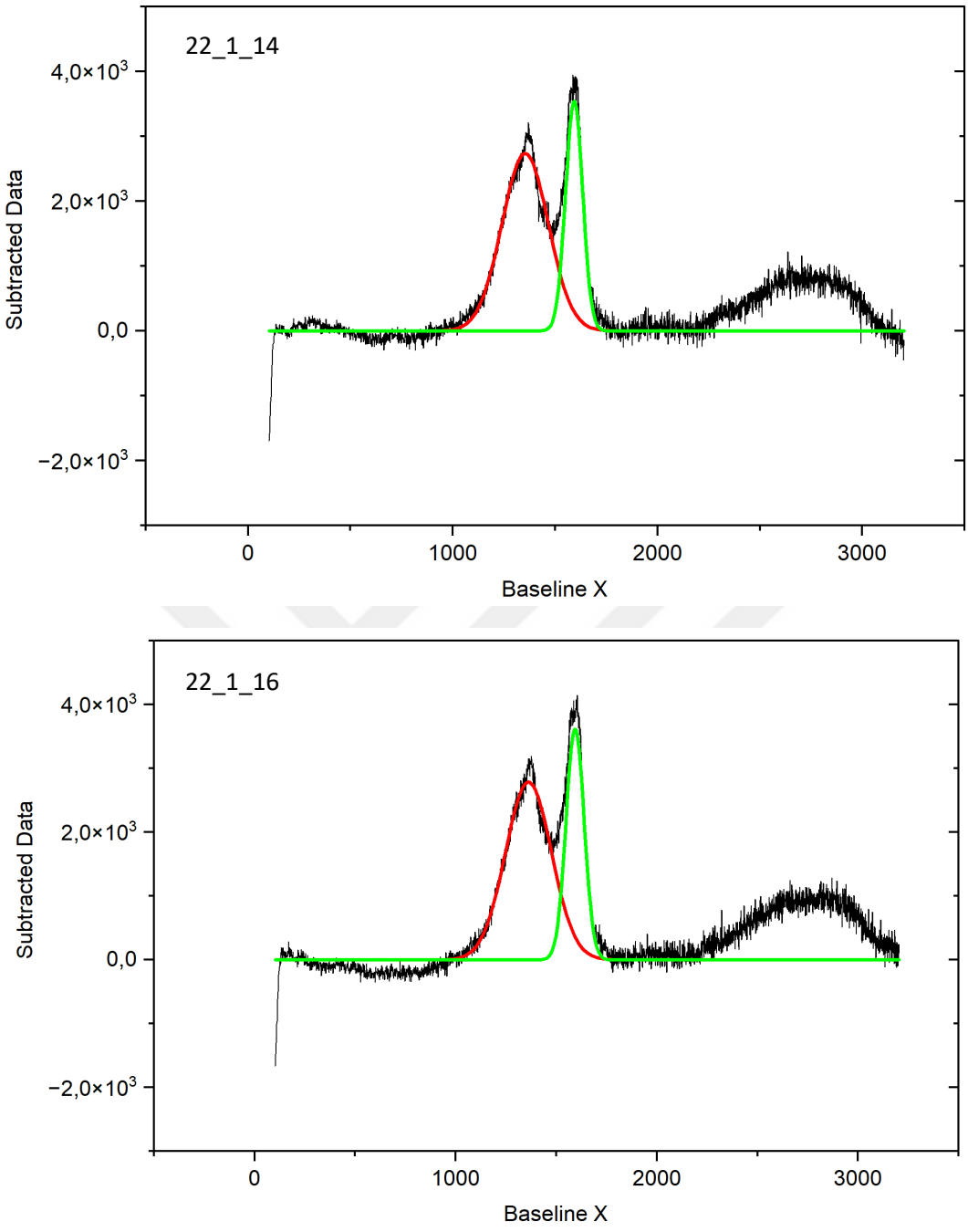

Plate 15. D1 and G peak parameters of samples from OriginPro.

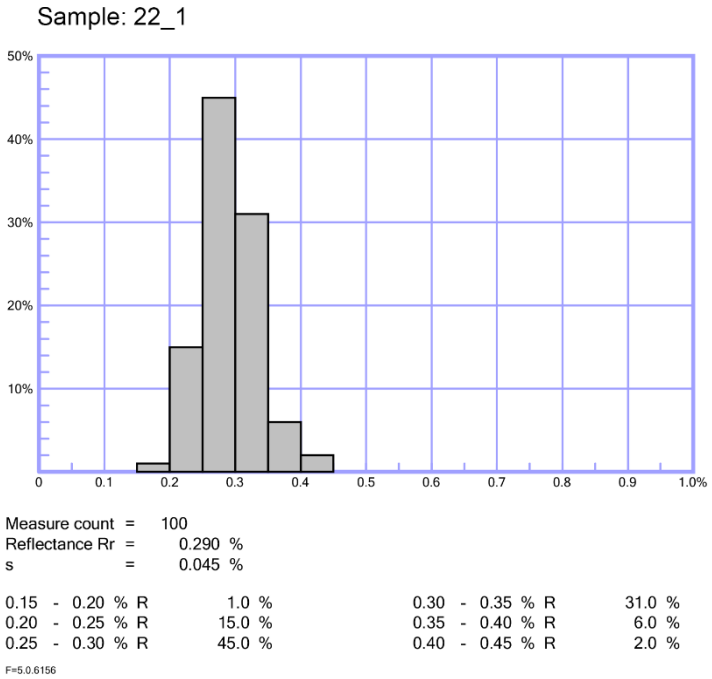

Plate 16. Histogram of the reflectance measurement of sample #1.

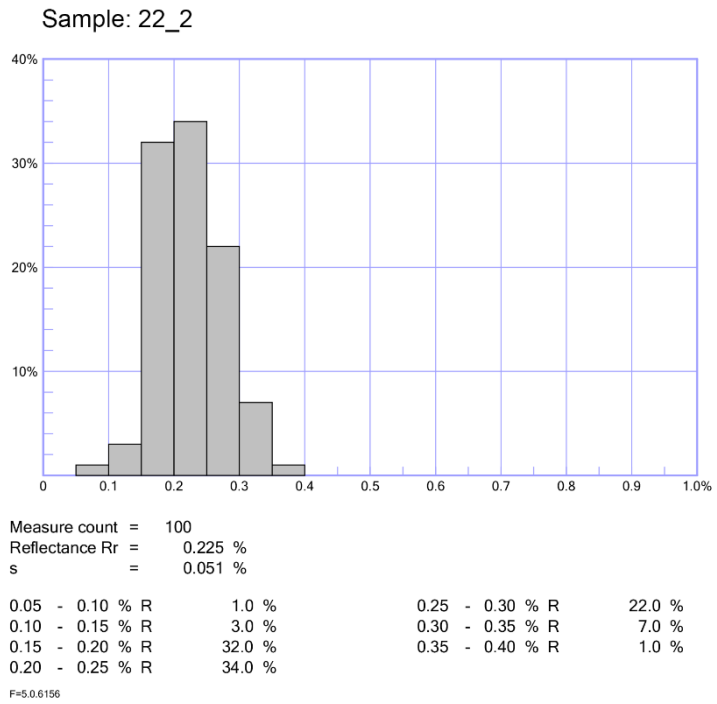

Plate 17. Histogram of the reflectance measurement of sample #2.

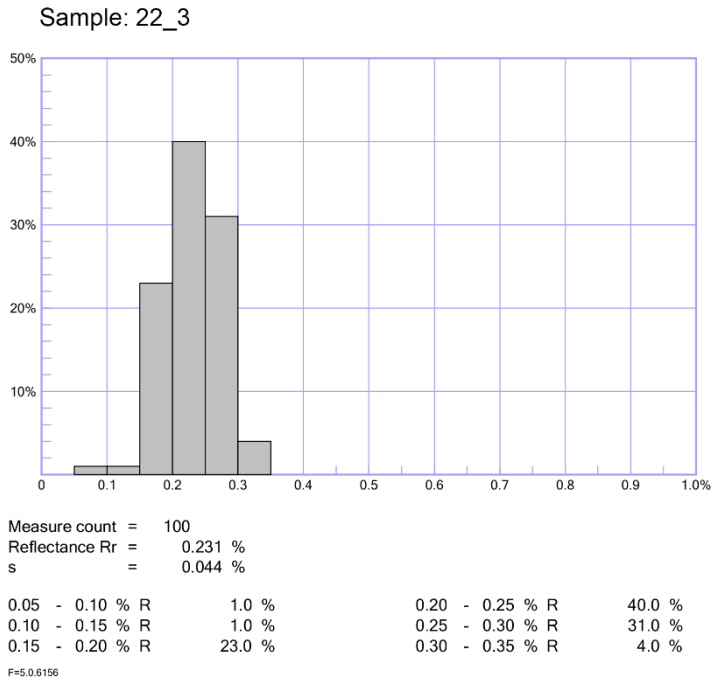

Plate 18. Histogram of the reflectance measurement of sample #3.

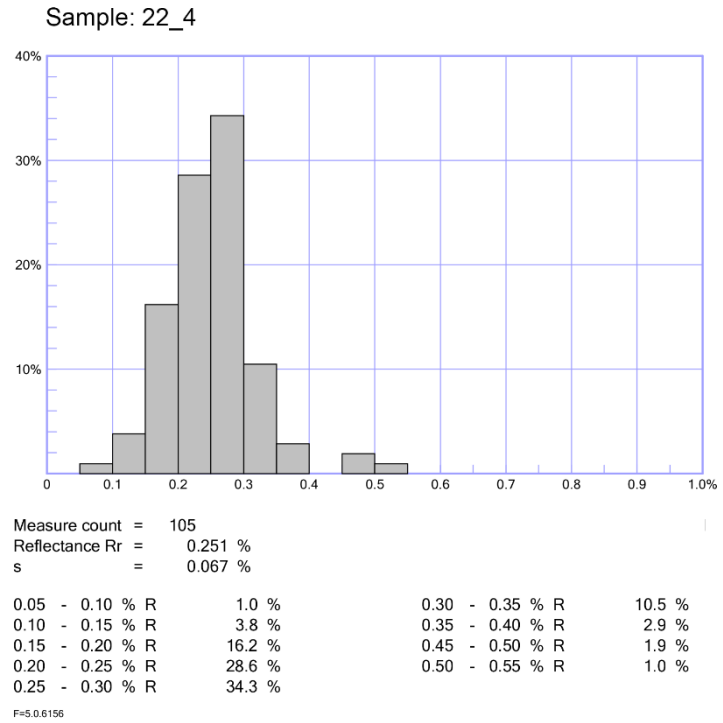

Plate 19. Histogram of the reflectance measurement of sample #4.